AD-A064 376 FACTORY MUTUAL RESEARCH CORP NORWOOD MASS F/G 1/2
PRESSURE MODELING OF VERTICALLY BURNING AIRCRAFT MATERIALS.(U)
JAN 79 R L ALPERT DOT-FAA77NA-4048
UNCLASSIFIED 0A0R8.BU FAA/RD-78/139 NL

1 OF 1
AD
A064376

END
DATE
FILMED
4-79
DDC

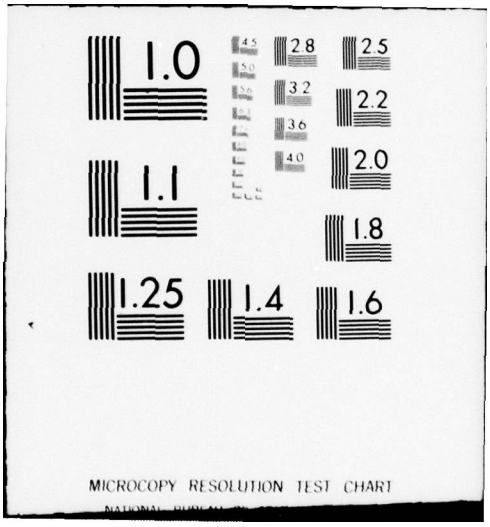
1.0
1.1
1.25
1.4
1.6
1.8
2.0
2.2
2.5
2.8
3.2
3.6
4.0
4.5
5.0
MICROCOPY RESOLUTION TEST CHART

Report No. FAA-RD-78-139

LEVEL II

PRESSURE MODELING OF VERTICALLY BURNING AIRCRAFT MATERIALS

R. L. Alpert

JANUARY 1979

FINAL REPORT

Prepared for

U.S. DEPARTMENT OF TRANSPORTATION
FEDERAL AVIATION ADMINISTRATION
Systems Research & Development Service
Washington, D.C. 20590

NOTICE

The United States Government does not endorse products or manufacturers. Trade or manufacturer's names appear herein solely because they are considered essential to the object of this report.

(14) ØAØR8.BU, RC78-BT-29

Technical Report Documentation Page

1. Report No. (17) (18) FAA/RD 78-139	2. Government Accession No.	3. Recipient's Catalog No. (12) 64p.
4. Title and Subtitle (6) PRESSURE MODELING OF VERTICALLY BURNING AIRCRAFT MATERIALS.		5. Report Date (11) Jan[redacted]979
		6. Performing Organization Code
7. Author(s) (10) R. L. Alpert		8. Performing Organization Report No. 0A0R8.BU; RC78-BT-29
9. Performing Organization Name and Address Factory Mutual Research Corporation 1151 Boston-Providence Turnpike Norwood, Massachusetts 02062		10. Work Unit No. (TRAIS) (15) 11. Contract or Grant No. DOT-FAA77NA-4048
12. Sponsoring Agency Name and Address U. S. Department of Transportation Federal Aviation Administration National Aviation Facilities Experimental Center Atlantic City, New Jersey 08405		(9) 13. Type of Report and Period Covered Final Rept. Octo[redacted]977- [redacted]h Jul[redacted]978 14. Sponsoring Agency Code ANA-420

15. Supplementary Notes

This report is additionally identified through the sponsor report No. FAA-NA-79-150. NH

16. Abstract

The possibility of evaluating relative rates of upward fire spread on aircraft cabin materials is investigated with small-scale models burned at elevated ambient air pressure. The modeling technique, which preserves the fluid Grashof number of the full-scale fire spread process, is verified in the first part of the study with vertical walls of polymethyl methacrylate (PMMA) fuel ignited at one atmosphere (full-scale) and at elevated absolute pressures (model) to 3.5 MPa (515 psia). In the second phase of the study, fifteen aircraft cabin samples are subjected to a small PMMA ignition source for a range of elevated ambient air pressures. Rates of upward fire spread, characterized by flame height exponential growth factors, are measurable for nearly all the aircraft cabin materials at absolute pressures from 1.18 MPa (165 psia) to 3.2 MPa (465 psia). Ranking of the materials by rate of upward fire spread is facilitated by the nearly two order of magnitude separation between highest and lowest growth factor at each pressure level. This ranking is found to be reasonably independent of pressure, enabling conservative predictions of upward spread behavior at one atmosphere to be made.

17. Key Words	18. Distribution Statement
Flame Spreading Aircraft Materials Fire Modeling Fire Dynamics Pressure Modeling	Unlimited Document is available to the U.S. public through the National Technical Information Service, Springfield, Virginia 22161

19. Security Classif. (of this report)	20. Security Classif. (of this page)	21. No. of Pages	22. Price
Unclassified	Unclassified		

Form DOT F 1700.7 (8-72) Reproduction of completed page authorized 1 33 300

79 02 08 058

METRIC CONVERSION FACTORS

Approximate Conversions to Metric Measures

Symbol	When You Know	Multiply by	To Find	Symbol
	LENGTH			
in	inches	*2.5	centimeters	cm
ft	feet	30	centimeters	cm
yd	yards	0.9	meters	m
mi	miles	1.6	kilometers	km
	AREA			
in^2	square inches	6.5	square centimeters	cm^2
ft^2	square feet	0.09	square meters	m^2
yd^2	square yards	0.8	square meters	m^2
mi^2	square miles	2.6	square kilometers	km^2
	acres	0.4	hectares	ha
	MASS (weight)			
oz	ounces	28	grams	g
lb	pounds	0.45	kilograms	kg
	short tons (2000 lb)	0.9	tonnes	t
	VOLUME			
tsp	teaspoons	5	milliliters	ml
Tbsp	tablespoons	15	milliliters	ml
fl oz	fluid ounces	30	milliliters	ml
c	cups	0.24	liters	l
pt	pints	0.47	liters	l
qt	quarts	0.95	liters	l
gal	gallons	3.8	liters	l
ft^3	cubic feet	0.03	cubic meters	m^3
yd^3	cubic yards	0.76	cubic meters	m^3
	TEMPERATURE (exact)			
°F	Fahrenheit temperature	5/9 (after subtracting 32)	Celsius temperature	°C

*1 in = 2.54 (exactly). For other exact conversions and more detailed tables, see NBS Misc. Publ. 286, Units of Weights and Measures, Price $2.25, SD Catalog No. C13.10:286.

Approximate Conversions from Metric Measures

Symbol	When You Know	Multiply by	To Find	Symbol
	LENGTH			
mm	millimeters	0.04	inches	in
cm	centimeters	0.4	inches	in
m	meters	3.3	feet	ft
m	meters	1.1	yards	yd
km	kilometers	0.6	miles	mi
	AREA			
cm^2	square centimeters	0.16	square inches	in^2
m^2	square meters	1.2	square yards	yd^2
km^2	square kilometers	0.4	square miles	mi^2
ha	hectares (10,000 m^2)	2.5	acres	
	MASS (weight)			
g	grams	0.035	ounces	oz
kg	kilograms	2.2	pounds	lb
t	tonnes (1000 kg)	1.1	short tons	
	VOLUME			
ml	milliliters	0.03	fluid ounces	fl oz
l	liters	2.1	pints	pt
l	liters	1.06	quarts	qt
l	liters	0.26	gallons	gal
m^3	cubic meters	35	cubic feet	ft^3
m^3	cubic meters	1.3	cubic yards	yd^3
	TEMPERATURE (exact)			
°C	Celsius temperature	9/5 (then add 32)	Fahrenheit temperature	°F

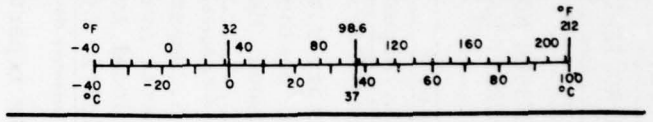

PREFACE

This report was sponsored by the Federal Aviation Administration, through a contract managed by Mr. Constantine P. Sarkos of the National Aviation Facilities Experimental Center (NAFEC), Atlantic City, New Jersey. The valuable advice and encouragement of Dr. Thor I. Eklund of NAFEC during the entire course of this work are gratefully acknowledged.

The support and patience of Dr. John deRis and Dr. Raymond Friedman of Factory Mutual Research Corporation are sincerely appreciated. Mr. Francis B. Kiley of FMRC ably performed the experiments described herein.

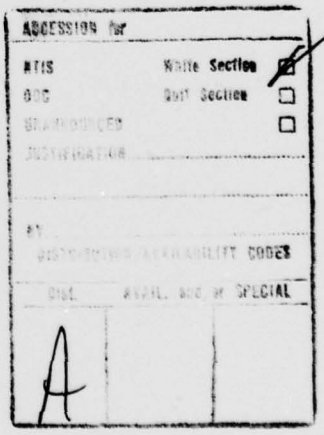

TABLE OF CONTENTS

	Page
INTRODUCTION	1
Purpose	1
Background	1
VERIFICATION OF MODELING OF UPWARD SPREAD	2
Pressure Modeling Technique	2
Experimental Arrangement	3
Experimental Results	5
Fire Spread	5
Upward Spread	8
Lateral Spread	14
Fire Radiance	14
Mass Loss	14
Modeling Validity	19
Analysis	24
APPLICATION OF MODELING TO AIRCRAFT MATERIAL FIRES	31
Modeling Techniques	31
Experimental Arrangement	31
Experimental Results	34
Upward Spread	37
Lateral Spread	42
Mass Loss	45
Analysis	45
SUMMARY OF RESULTS	53
CONCLUSIONS	54
REFERENCES	55

LIST OF FIGURES

Figure		Page
1	Schematic Diagram of PMMA Wall	4
2	Typical Photograph of Upward Fire Spread on Model PMMA Wall at Absolute Pressure of 1.1 MPa (11 atm)	6
3	Typical Photograph of Upward Fire Spread on Prototype PMMA Wall at One Atmosphere	7
4	Pyrolysis Zone Height for Model	9
5	Flame Height for Model	10
6	Flame and Pyrolysis Height for Prototype	11
7	Exponential Growth Factor for Pyrolysis Zone Height	12
8	Exponential Growth Factor for Flame Height	13
9	Maximum Width of Pyrolysis Zone for Models	15
10	Maximum Width of Pyrolysis Zone for Prototype	16
11	Flame and Fuel Radiance for Model	17
12	Fuel Burning Rate for Model	18
13	Correlation of Pyrolysis Zone Height	20
14	Correlation of Flame Height	21
15	Correlation of Maximum Width of Pyrolysis Zone	22
16	Correlation of Radiance Measurements for Model	23
17	Correlation of Burning Rates for Model	25
18	Exponential Growth Factor for Thermally Thick PMMA	26
19	Schematic Diagram of Aircraft Material in Fuel Holder	33
20	Typical Photograph of Upward Fire Spread on Aircraft Material	37
21	Examples of Flame Height for Complete Fire Spread	40
22	Examples of Flame Height for Incomplete Fire Spread	41
23	Examples of Maximum Flame Width	44
24	Examples of Fuel Mass Loss	47
25	Predicted Exponential Growth Factor for Thermally Thin Materials	53

LIST OF TABLES

Table		Page
1	Description of Aircraft Samples	37
2	Aircraft Samples with Incomplete Upward Spread	39
3	Upward Spread Growth Factors for NAFEC Samples	42
4	Characteristic Times for Lateral and Upward Fire Spread on NAFEC Samples	45
5	Peak Burning Rates of NAFEC Samples	48
6	Correlation of Upward Spread Growth Factors: NAFEC Samples Assumed Thermally Thin	50
7	Correlation of Upward Spread Growth Factors: NAFEC Samples Assumed Thermally Thick	51

LIST OF SYMBOLS

d	flame zone thickness normal to wall
k	flame radiation absorption coefficient
L_m	radiation mean-beam-length
$\dot{m}$	fuel burning rate
$\dot{m}''$	fuel mass flux
$\dot{m}''_o$	reference fuel mass flux at one atmosphere
N	radiance measured along axis normal to fuel surface
p	absolute air pressure
p_o	absolute atmospheric air pressure
$\dot{q}''$	net heat flux to fuel
$\dot{q}''_c$	convective heat flux from flames
$\dot{q}''_f$	radiant heat flux from flames
$\dot{q}''_{rr}$	reradiant heat loss from fuel
t	time
T_g	flame radiation temperature
T_p	fuel pyrolysis temperature
T_{po}	fuel pyrolysis temperature at one atmosphere
U_f	lateral spread rate of flame zone
V_f	upward spread rate of flame zone
V_p	upward spread rate of pyrolysis zone
W_f	flame zone width
W_{fm}	maximum flame zone width
W_o	total width of exposed fuel
W_p	pyrolysis zone width
W_{pm}	maximum pyrolysis zone width
x_f	flame zone height
x_p	pyrolysis zone height

Greek Symbols

α	reradiation constant, between zero and unity
σ	Stefan-Boltzman constant

INTRODUCTION

PURPOSE

The purpose of this project is first to verify that the process of vertical upward fire spread can be pressure modeled for thermally thick polymethyl methacrylate (PMMA) and then to apply this modeling technique to measuring the relative flammabilities of 15 types of aircraft materials.

BACKGROUND

The rate of vertical, upward fire spread on a material is generally higher than that for any other fuel orientation, often leading to an accelerating flame front with increasing fuel height. As a result, this spread rate is usually difficult to measure with precision, even in the laminar-flow region below a fuel height of about 0.2 m (see Reference 14), where flame propagation is still slow. Furthermore, upward fire spread may be inadvertently enhanced if too much fuel above the ignition source is preheated. Despite these difficulties, it is generally recognized that various aspects of the process of upward fire spread can be used to qualitatively assess the fire hazard of a material. Successful modeling of this spread process would therefore be highly desirable.

Pressure modeling is a technique for physically modeling the process of transient fire growth in solid fuels. The technique, first evaluated in reference 1, involves the use of high air pressure and small scale physical dimensions to simulate the Reynolds and Froude numbers characteristic of large-scale fires. At an absolute air pressure of 3.1 MPa (465 psia) for instance, one-tenth scale models of fuels and all other dimensions can be used. A detailed review of pressure modeling results was recently reported in reference 2. In the latter reference, it is shown that the modeling technique should be used with caution whenever thermal radiation from solid surfaces has a dominant effect on fire growth or whenever the thickness of radiating gases (such as flame zones or smoke) is so excessive as to approach optically thick (black body) conditions at the high air pressure of the model test.

As demonstrated in reference 2, the process of steady burning of vertical polymethyl methacrylate (PMMA) surfaces up to 3.6 m (12 ft) high can be modeled quite accurately. Whether such modeling success would extend to the very important process of upward fire spread on a vertical fuel surface was not previously investigated. One would expect pressure modeling of upward fire spread to be as valid as the modeling of steady burning if the spread process is simply a succession of steady burning states.

The present study provides clear evidence that upward fire spread on vertical PMMA walls can indeed be pressure modeled. Conditions necessary for modeling fuels other than PMMA are also discussed. This information is then applied to the practical problem of determining the full-scale upward fire spread hazard of fifteen aircraft cabin materials chosen by NAFEC. Although the thickness of the model aircraft materials is identical to that used at full-scale, instead of being reduced by the appropriate scaling factor, the measured upward spread rates have been ranked. This ranking by upward spread hazard is found to be essentially independent of ambient air pressure.

VERIFICATION OF MODELING OF UPWARD SPREAD

PRESSURE MODELING TECHNIQUE

The scheme for pressure modeling fires, as explained in reference 1 and verified in references 1, 2 and 3 for PMMA and pine-wood fuels, requires the reduction of all length scales as the minus 2/3 power of absolute air pressure. As a result, gas phase Reynolds and Froude numbers (ratios of inertial to viscous forces and of inertial to buoyant forces, respectively) will be preserved as pressure is increased and scale reduced. Furthermore, solid phase thermal response and vaporization will also model full-scale phenomena, through preservation of the Fourier Number (ratio of characteristic burning time to thermal time scales), but on a time scale which is reduced as the minus 4/3 power of absolute air pressure, p.

If a fuel is sufficiently thick, the thermal wave (of increased solid temperature) will not penetrate through to the fuel back surface while a fire on the front surface is spreading or burning. For such a "thermally thick" fuel, the rate of fire spread will not depend on the fuel thickness but only on the characteristic distance traversed by the fire divided by the characteristic spread time. Since distances should be reduced as $p^{-2/3}$ and solid phase response times as $p^{-4/3}$, spread rates over thermally thick solids should increase as the 2/3 power of absolute air pressure.

The modeling concepts discussed above should be generally valid as long as the heat transfer mode (e.g. from flames to the fuel surface) is predominantly by convection and conduction rather than by radiation. However, it is now well-known (see references 4 and 5) that thermal radiation is the dominant heat transfer mechanism in nearly all real fire situations. Under such conditions of non-negligible thermal radiation, the pressure modeling scheme requires detailed verification before being applied to new classes of fuels or types of fuel geometries. For this reason, measurements of upward fire spread rates on vertical PMMA walls are made during the verification phase of the present study for a wide range of ambient air pressure, including normal atmospheric pressure. PMMA fuel is used since the vaporization and combustion mechanisms for this fuel are relatively simple and well understood. Furthermore, the transparency of PMMA allows the boundary of the vaporization zone to be observed during the upward spread process.

EXPERIMENTAL ARRANGEMENT

In the verification experiments, the rate of spread of a PMMA vertical wall fire is studied with models at elevated pressure and with a large-scale prototype at one atmosphere. Model tests are conducted in a vessel at FMRC of 1.22 m I.D., 2.7 m^3 volume, and 3.8 MPa (558 psia) maximum working pressure. Combustion products are well above the flame zone of all the model fires reported due to stratification and an adequate vessel interior volume. Further details about the pressure vessel may be found in reference 3. A full-scale prototype fire is conducted in an FMRC fire-test building with a ceiling height 5 times that of the PMMA fuel and comparable wall to wall distances.

The fuel is ignited at a single small point with roughly the minimum energy needed to cause self-sustained fire spread. This point ignition source is chosen (rather than a line source across the base of the wall) to enhance reproducibility and minimize any effect of ignition mode on the subsequent rate of fire spread. For all experiments at elevated pressure, the ignition energy is provided by an ordinary, round, wooden toothpick, extending out about 50.8 mm from a hole where the toothpick is forced into the PMMA surface. Details of this ignition scheme are illustrated in a schematic in Figure 1. At one atmosphere, a propane torch is applied to the PMMA surface just long enough to initiate self-sustained combustion.

For the sake of convenience, all of the model walls burned at elevated pressure are of a uniform size (see Fig. 1), 0.305 m high and 12.7 mm thick, with edges made inert by ceramic paper glued to the PMMA. The ceramic paper extends for one-sixth the wall width beyond the PMMA surface to form side walls. The one-atmosphere prototype wall is 1.8 m high and geometrically similar to the models, except for having a thickness of 38 mm. In all cases, the PMMA walls are certainly thermally thick, since the thermal wave thickness at one atmosphere is no more than 18 mm while the amount of PMMA consumed is no more than about 10 mm during fire spread. Thus, at the conclusion of fire spread, the thermal wave has penetrated less than 28 mm. For the models, thermal wave penetration is reduced as $p^{-2/3}$, to a value usually much less than the actual PMMA thickness.

Total fuel mass loss in the pressure vessel is obtained from a conventional load transducer coupled to the platform on which the PMMA wall is mounted (see ref. 3). Unfortunately, the mass resolution of the combined load transducer-digital data acquisition system is only about one gram while just a few grams of fuel are lost during fire spread. Calculated burning rates corresponding to the fire spread process thus have only order of magnitude accuracy.

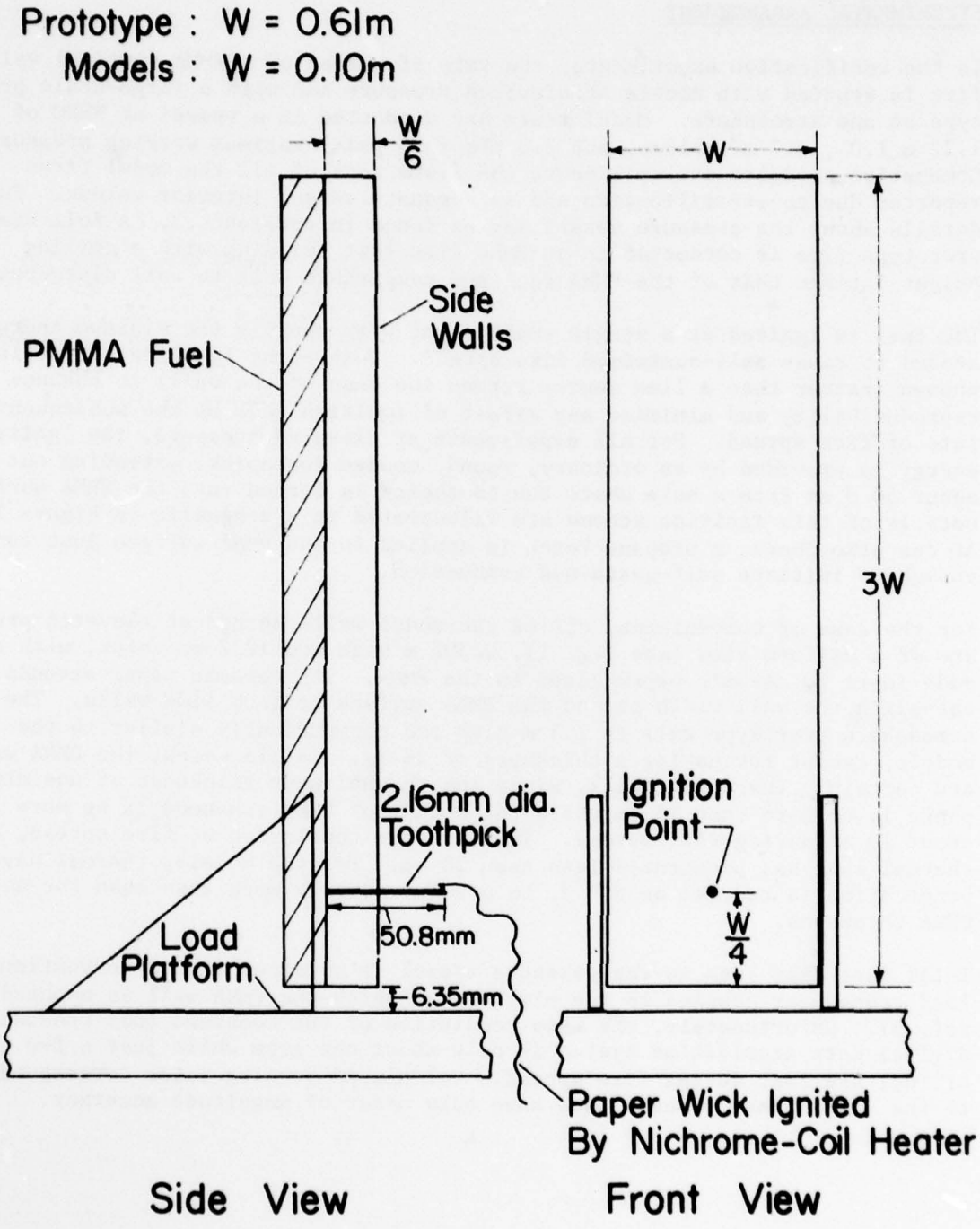

Figure 1: Schematic Diagram of PMMA Wall

Measurements of combined flame and fuel surface radiance (radiative power per unit solid angle per unit area) in the pressure vessel are obtained with a narrow angle (total angle 1.2 degrees), optically chopped radiometer. This instrument operates in conjunction with an amplifier locked-in to the actual rotational frequency of the mechanical chopper. The detector of the chopped infrared radiation is a black, thermopile-type (Sensors, Inc.) operating at normal atmospheric pressure by means of a sealed enclosure, Irtran II window and a vent line connected to the ambient atmosphere outside the vessel. Further details on the construction of the vessel radiometer are given in references 2 and 6. Mass loss and radiance measurements were not obtained during the full-scale fire spread experiment.

Rates of upward fire spread and the instantaneous position of both the pyrolysis and flame zones are derived from 35 mm photographs taken from behind the burning PMMA walls. A motorized camera with the capability for taking up to 5 frames per second is used to visualize the advance up the wall of the flame followed by the onset of surface bubbles which characterize the beginning of fuel pyrolysis (or vaporization). The transparency of the PMMA allows this "bubble front" to be seen as a sudden change in the character of the soot deposited on the PMMA surface by the flame zone. Time intervals are obtained during the fire spread process by photographed digital clocks which are synchronized with mass loss and radiance measurements. All photographic information of interest is converted to a digital format by a hand-held cursor moved along the photographic image, which has been projected onto a large, calculator-coupled sensing plate. Through experience, it has been found that 35 mm still photography (or some larger film format) is necessary to give enough resolution of the fuel pyrolysis boundary to make the digitization process successful.

EXPERIMENTAL RESULTS

FIRE SPREAD. A typical photograph of upward spread from a point ignition at an elevated pressure of 1.1 MPa (165 psia) is shown in Figure 2 while the full-scale prototype fire spread at one atmosphere is shown in Figure 3. Note that the region where the fuel has begun to vaporize is shaped like an elongated teardrop since rates of upward spread are so much greater than those for either lateral or downward spread. Note also that the flame zone appears to be fully turbulent, which occurs once the total fuel vaporization height at one atmosphere is only about 0.2 m (see reference 4). In a previous study of fire spread up PMMA walls from a point ignition, Hansen and Sibulkin (see reference 7) obtained pyrolysis regions shaped very much like those in Figures 2 and 3, even though the scale of the fuel used in their experiments (0.23 m maximum PMMA height, at one atmosphere) probably resulted in mainly laminar flames.

Measurements are obtained from photographs similar to those in Figures 2 and 3 of the total height of both the pyrolysis zone and the flame zone. The pyrolysis zone is defined by the inner edge of the teardrop-shaped soot line, which merges with the lower boundary of the flame zone (see Figure 2) in a semicircular region. This latter region is formed by the very slow, downward fire spread from the ignition point. While the shape of the pyrolysis zone changes gradually with time, the upper portion of the flame zone fluctuates a great deal. A visual estimate of a spatially averaged flame tip position is made to compensate for this fluctuation.

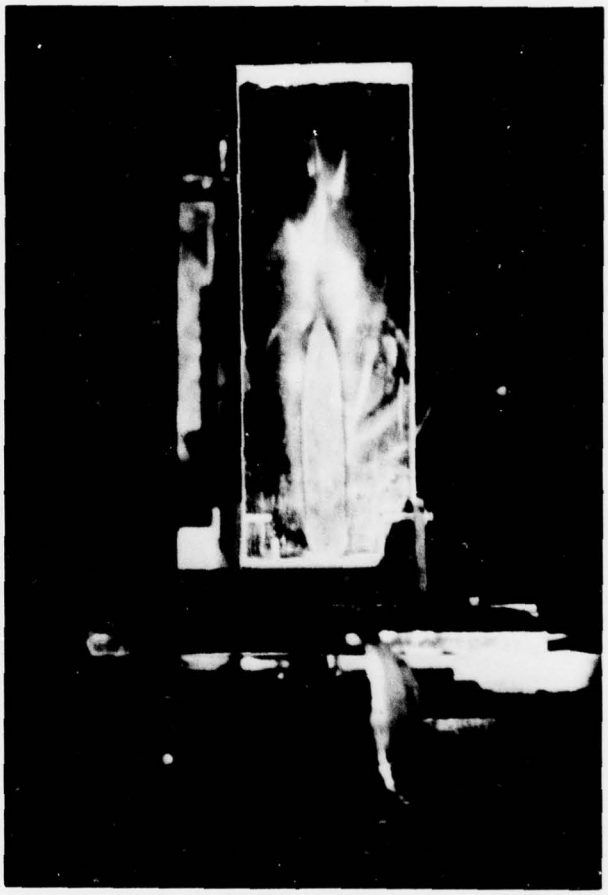

FIGURE 2. TYPICAL PHOTOGRAPH OF UPWARD FIRE SPREAD ON MODEL PMMA WALL AT ABSOLUTE PRESSURE OF 1.1 MPa (11 atm)

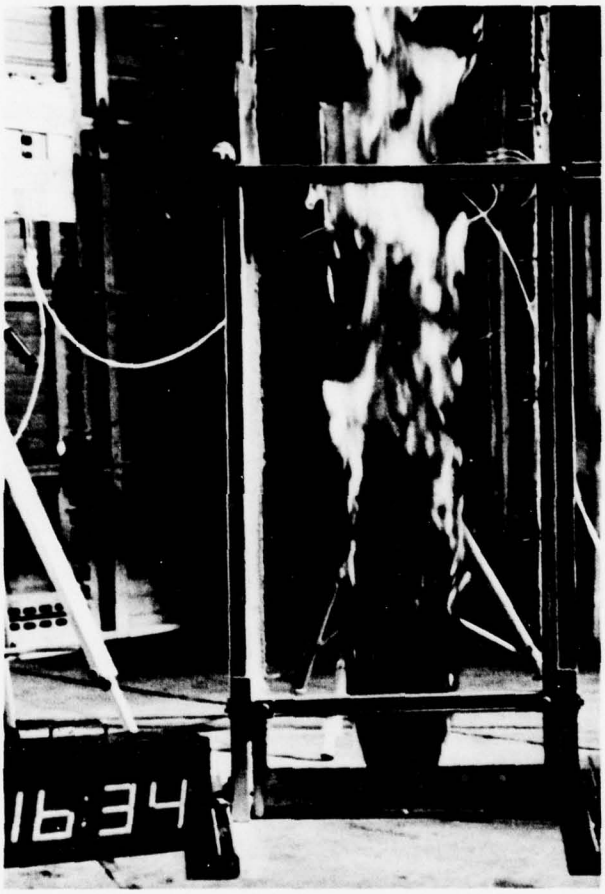

FIGURE 3. TYPICAL PHOTOGRAPH OF UPWARD FIRE SPREAD ON PROTOTYPE PMMA WALL AT ONE ATMOSPHERE

UPWARD SPREAD. Total pyrolysis zone height, x_p, and flame height, x_f, are shown plotted in Figures 4 and 5 as a function of time, t, from ignition for the model walls and in Figure 6 for the full-scale prototype. Since the exact time origin is not precisely controllable for the model experiments, all times at elevated pressure have been shifted to yield agreement with the initial measurement of full-scale pyrolysis height. It should also be noted that the data in Figures 4 and 5 represent the results of two separate experiments at each pressure. Good reproducibility is evident.

It can be seen in Figures 4, 5 and 6 that log x_p or log x_f is almost linearly dependent on t, implying an exponential growth with time of pyrolysis or flame height. This result is consistent with computed regression coefficients of 0.96, 0.98 and 0.95 for "least squares" linear, exponential and power law ($x = At^n$) best fits to pyrolysis height vs time data, respectively, for the prototype fire. Corresponding average values of the linear, exponential and power law regression coefficients at elevated pressure are 0.951, 0.992 and 0.990. The exponential fit is thus clearly best for the full-scale fire and marginally better for the model fires.

Because of the linear dependence of log x on time, the upward spread velocity, V, is given by the following:

$$V = \frac{dx}{dt} = Bx \qquad (1)$$

Thus, the spread velocity is simply proportional to the height, x, and the proportionality factor, B, is the slope of the lines in Figures 4 to 6.

The ratios V_p/x_p and V_f/x_f have been plotted in Figures 7 and 8 as a function of the ratio of ambient pressure to that at one atmosphere, p/p_o. The value of V/x, or B, is the exponential growth factor in the "best" fit to the x-t data for each experiment.

Figures 7 and 8 show that the growth factor increases by two orders of magnitude as the ambient pressure is elevated from one atmosphere to 35 atmospheres (3.5 MPa, or 514 psia). This corresponds to a reduction in the characteristic time for doubling the flame or pyrolysis height, x, from about 290 seconds to 2.9 seconds. The doubling time of 290 seconds at one atmosphere, it should be noted, is significantly greater than that found when upward spread is initiated from a line ignition source at the base of the PMMA wall, instead of from a point source. As shown by the measurements in reference 4, the doubling time with a line ignition is only 178 seconds, implying that spread velocities are about 60% higher for that case. This difference is due to the greater air entrainment, and hence shortened flames, with a point ignition since the narrow pyrolysis region allows greater access to ambient air. For a line ignition, pyrolysis is occurring across the entire width of the wall, leading to higher flames and higher spread velocity.

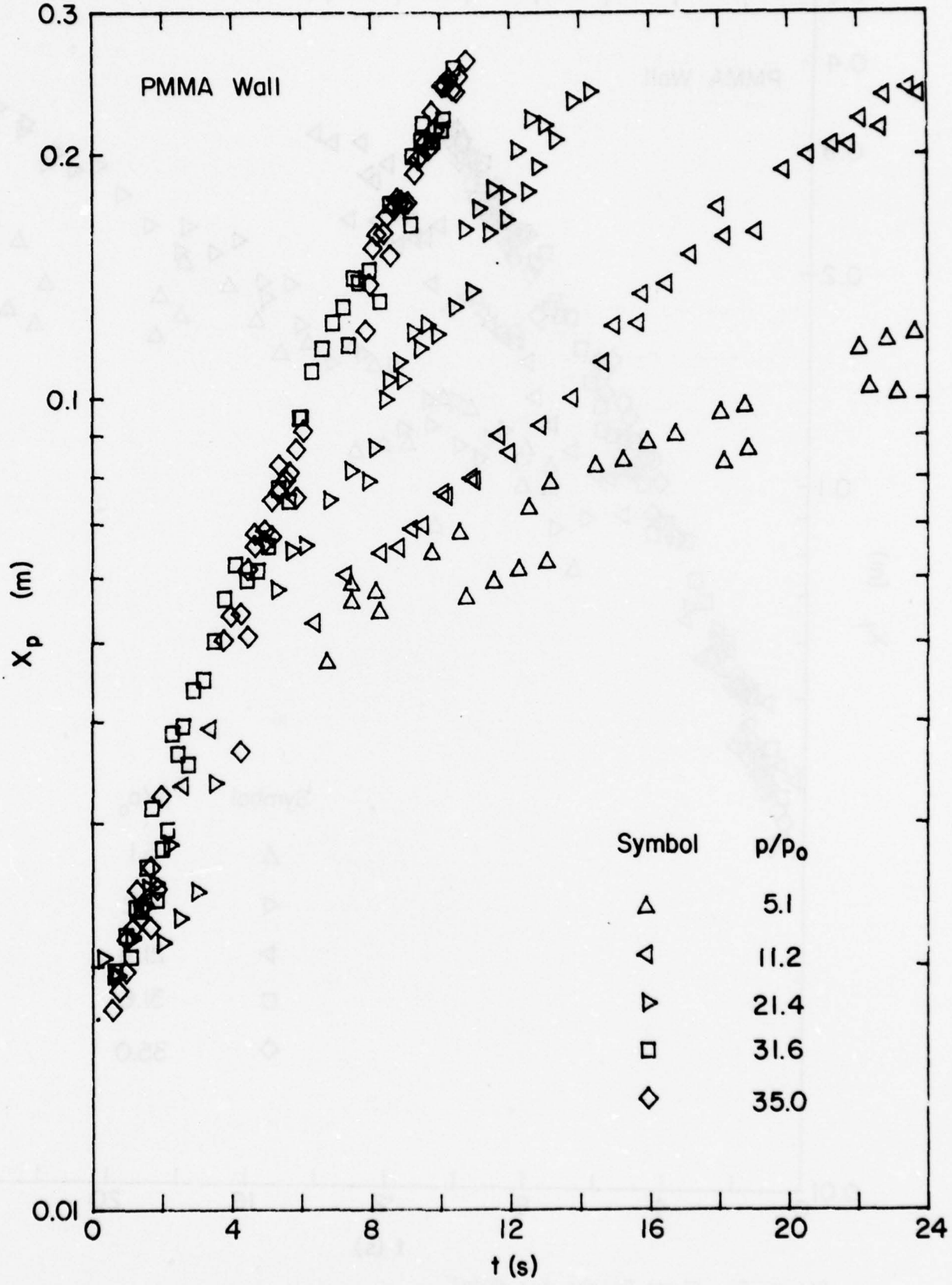

Figure 4: Pyrolysis Zone Height for Model

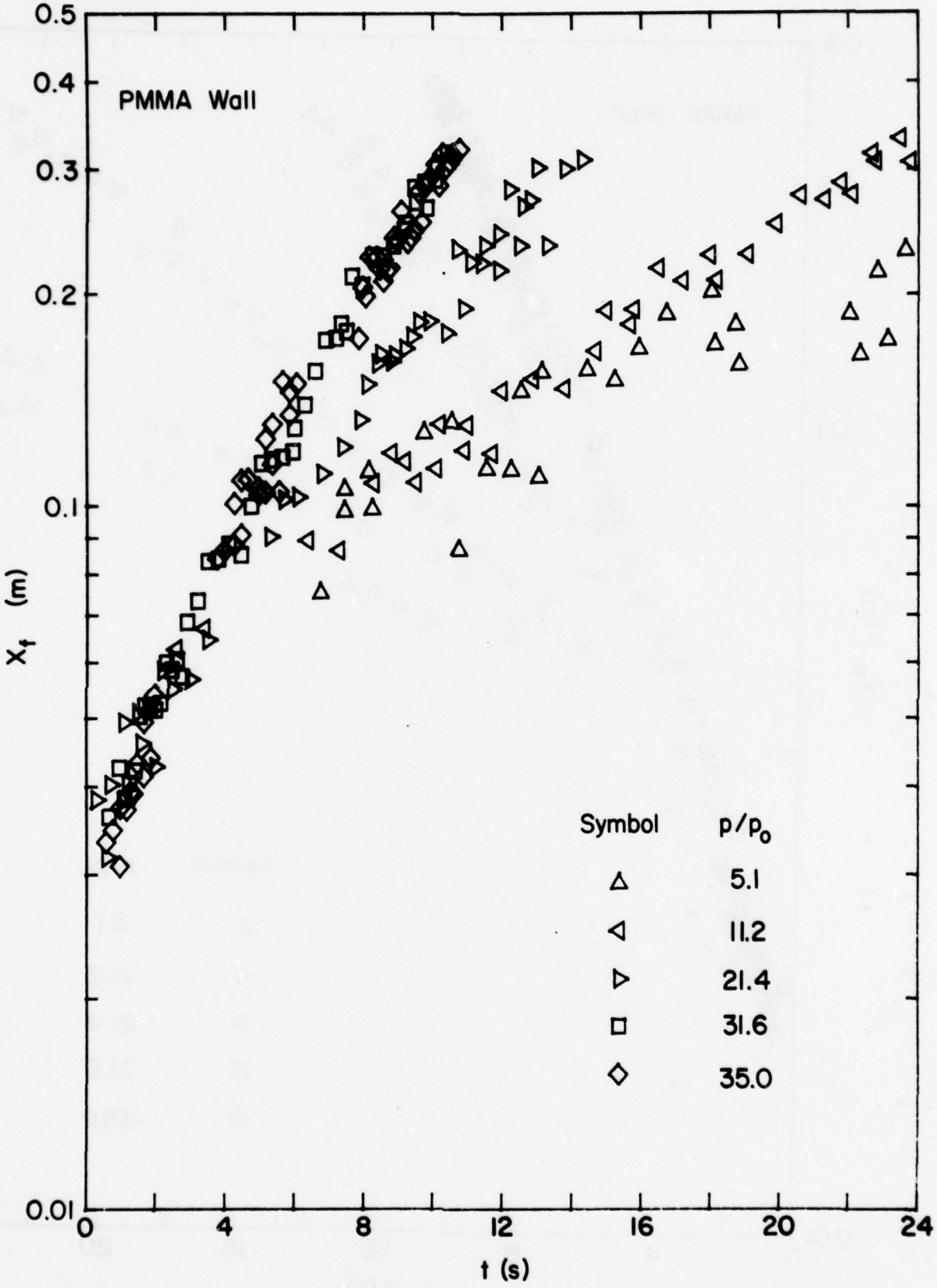

Figure 5: Flame Height for Model

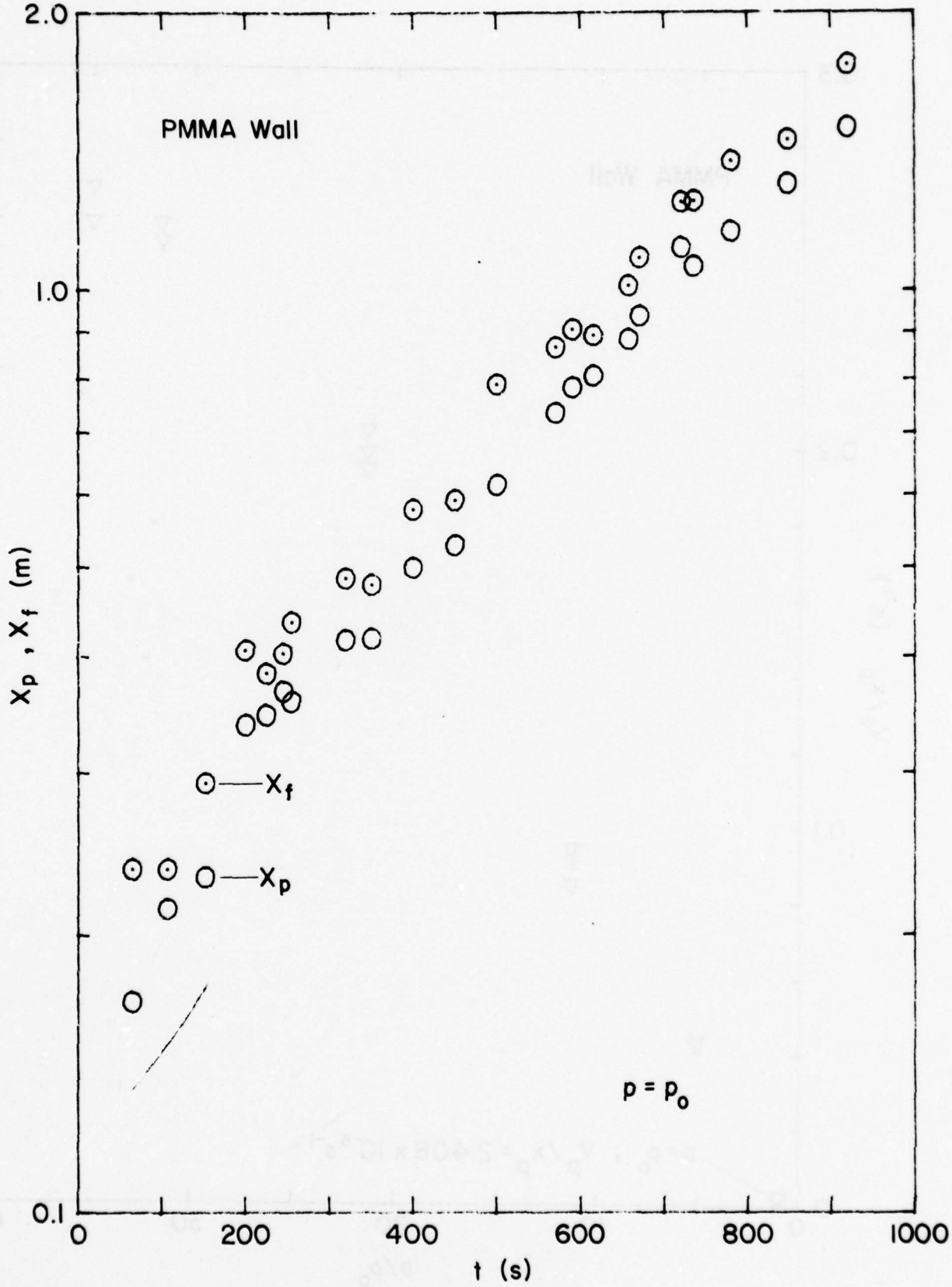

Figure 6: Flame and Pyrolysis Height for Prototype

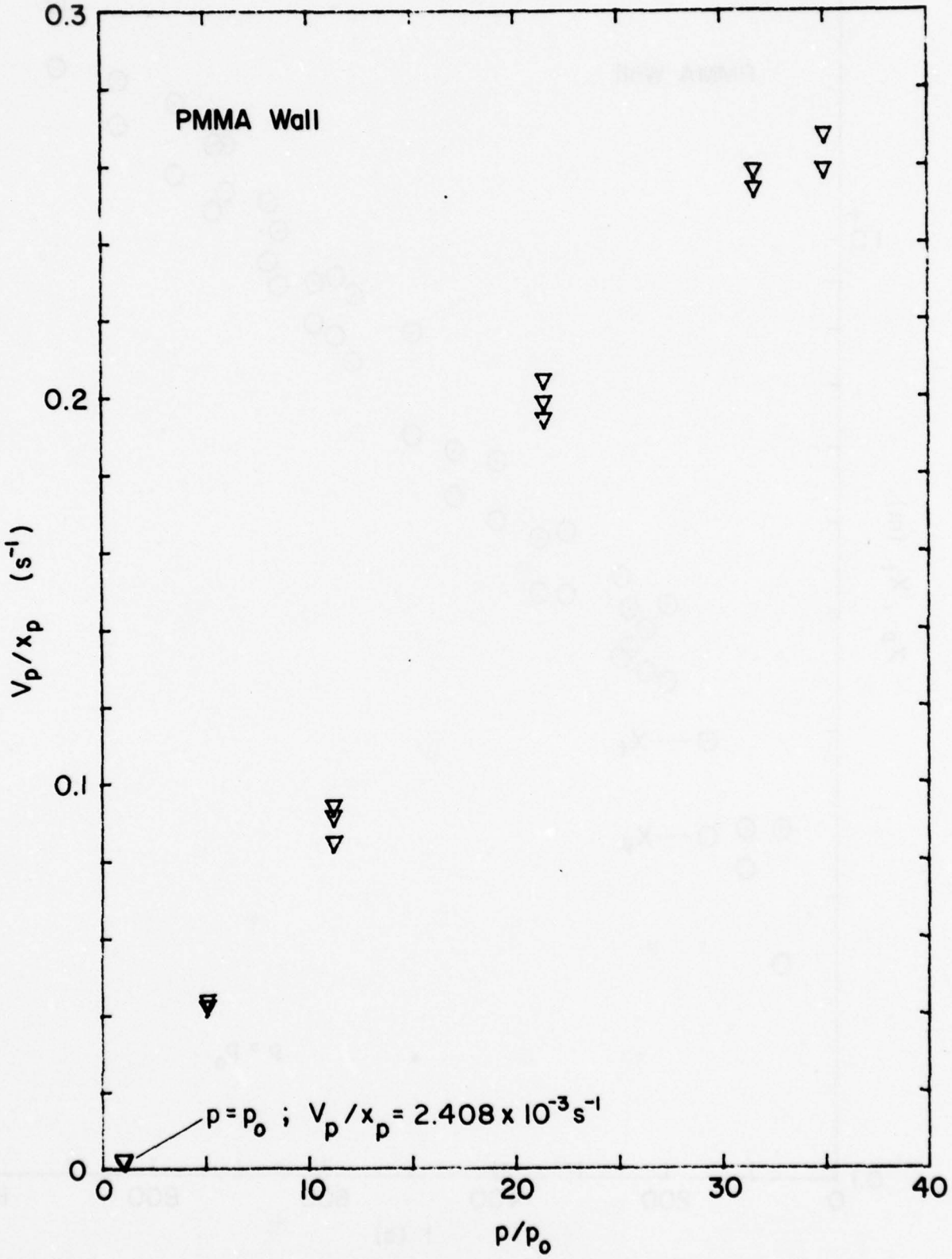

Figure 7: Exponential Growth Factor for Pyrolysis Zone Height

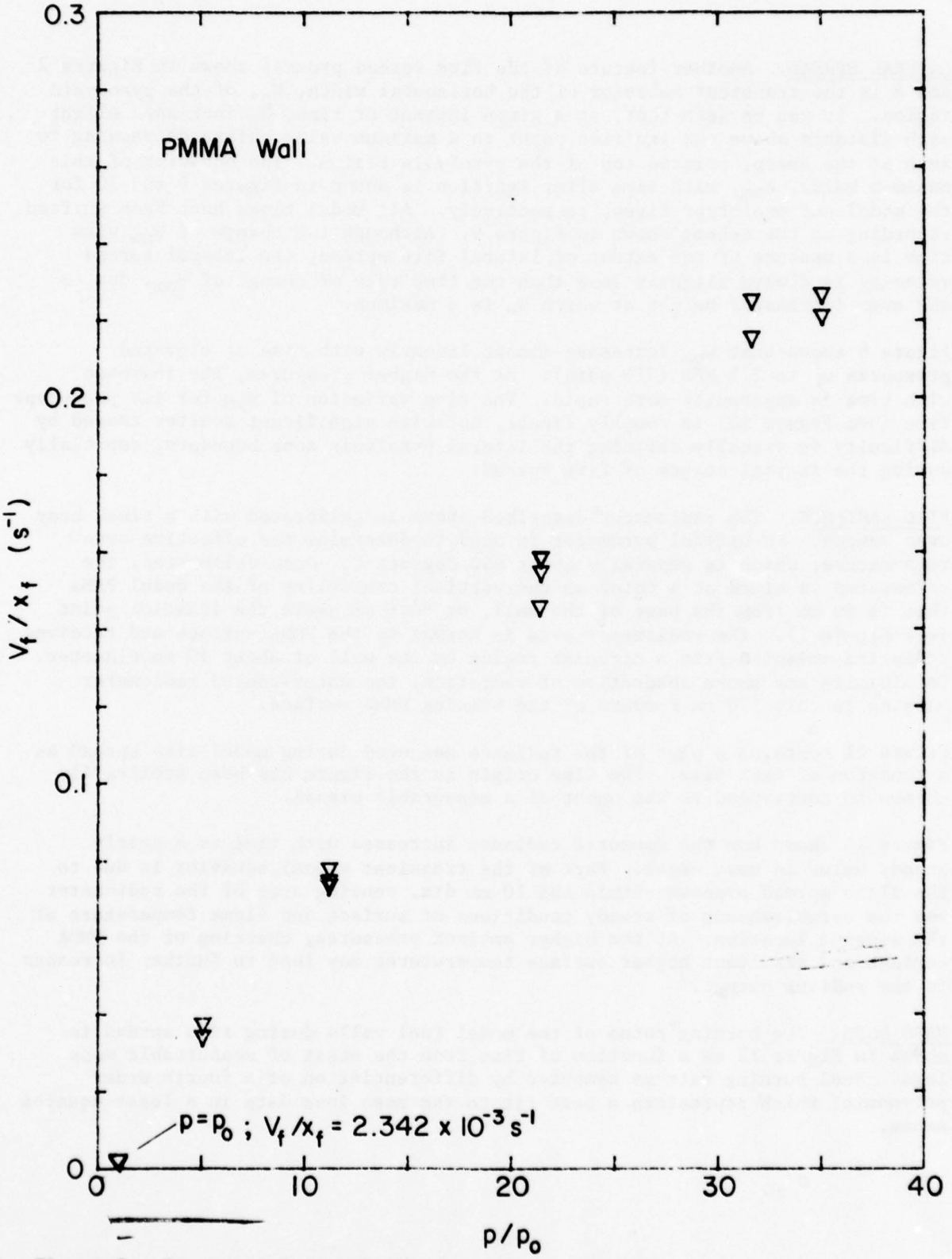

Figure 8: Exponential Growth Factor for Flame Height

LATERAL SPREAD. Another feature of the fire spread process shown in Figures 2 and 3 is the transient behavior of the horizontal width, W_p, of the pyrolysis region. It can be seen that, at a given instant of time, W_p increases slightly with distance above the ignition point to a maximum value before decreasing to zero at the sharp, pointed top of the pyrolysis region. The behavior of this maximum value, W_{pm}, with time after ignition is shown in Figures 9 and 10 for the model and prototype fires, respectively. All model times have been shifted according to the scheme shown in Figure 9. Although the change of W_{pm} with time is a measure of the extent of lateral fire spread, the lateral spread velocity is always slightly less than the time rate of change of W_{pm}, due to the ever increasing height at which W_p is a maximum.

Figure 9 shows that W_{pm} increases almost linearly with time at elevated pressures up to 2.1 MPa (315 psia). At the higher pressures, the increase with time is apparently more rapid. The time variation of W_{pm} for the prototype fire (see Figure 10) is roughly linear, but with significant scatter caused by difficulty in visually defining the lateral pyrolysis zone boundary, especially during the initial stages of fire spread.

FIRE RADIANCE. The radiometer described above is calibrated with a black body oven source. An optical pyrometer is used to determine the effective oven temperature, which is generally about 850 degrees C. Once calibrated, the radiometer is aimed at a point on the vertical centerline of the model PMMA that is 90 mm from the base of the wall, or 64.6 mm above the ignition point (see Figure 1). The radiometer axis is normal to the PMMA surface and receives radiative emission from a circular region on the wall of about 10 mm diameter. To minimize any smoke absorption of radiation, the water-cooled radiometer housing is only 170 mm forward of the burning PMMA surface.

Figure 11 contains a plot of the radiance measured during model fire spread as a function of test time. The time origin in the figure has been arbitrarily chosen to correspond to the onset of a measurable signal.

Figure 11 shows how the measured radiance increases with time to a nearly steady value in most cases. Part of the transient signal behavior is due to the flame spread process within the 10 mm dia. sensing area of the radiometer and the establishment of steady conditions of surface and flame temperature at the sensing location. At the higher ambient pressures, charring of the PMMA surface and resultant higher surface temperatures may lead to further increases in the radiant output.

MASS LOSS. The burning rates of the model fuel walls during fire spread is shown in Figure 12 as a function of time from the onset of measureable mass loss. Fuel burning rate is computed by differentiation of a fourth order polynomial which represents a best fit to the mass loss data in a least squares sense.

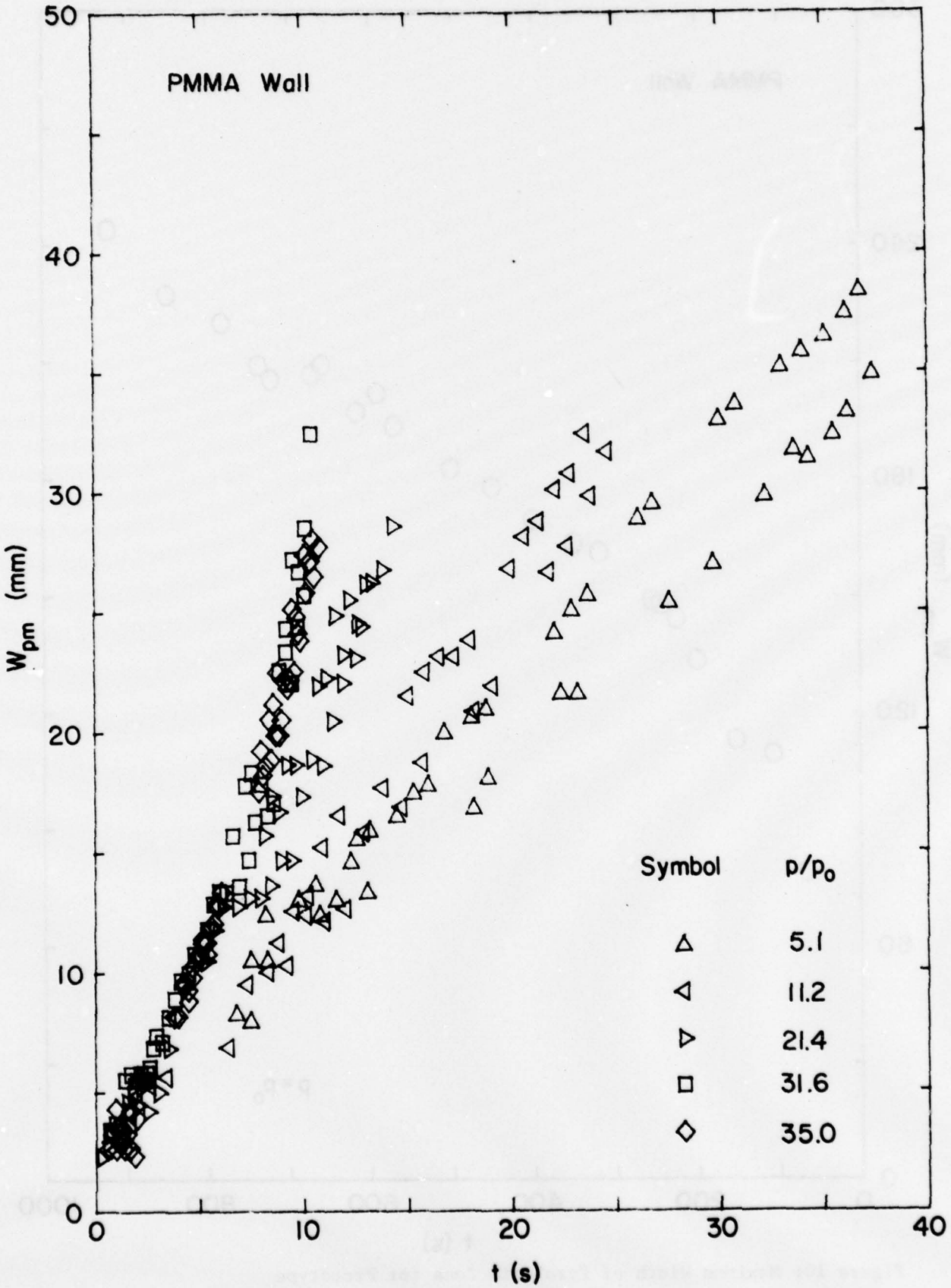

Figure 9: Maximum Width of Pyrolysis Zone for Models

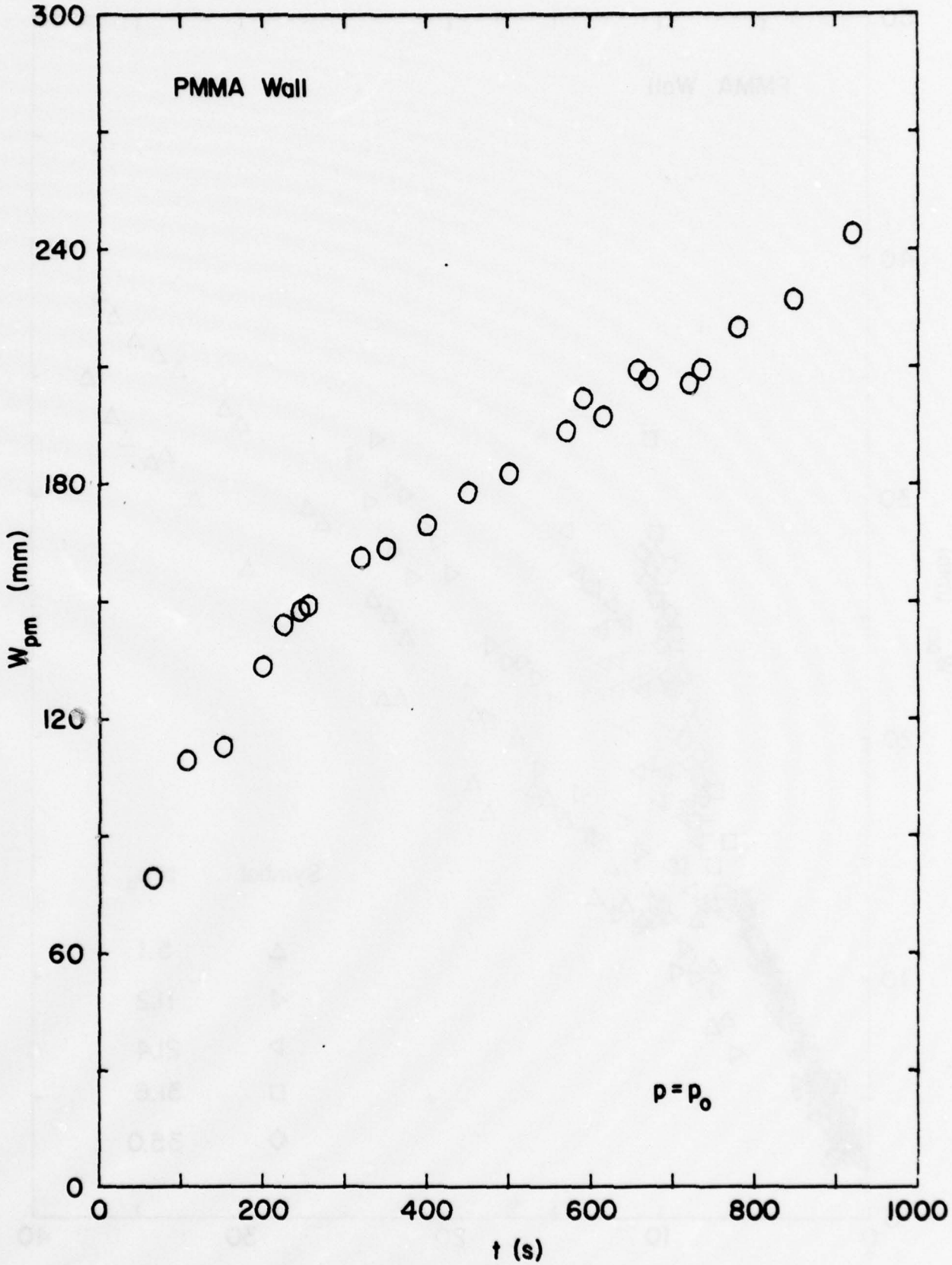

Figure 10: Maximum Width of Pyrolysis Zone for Prototype

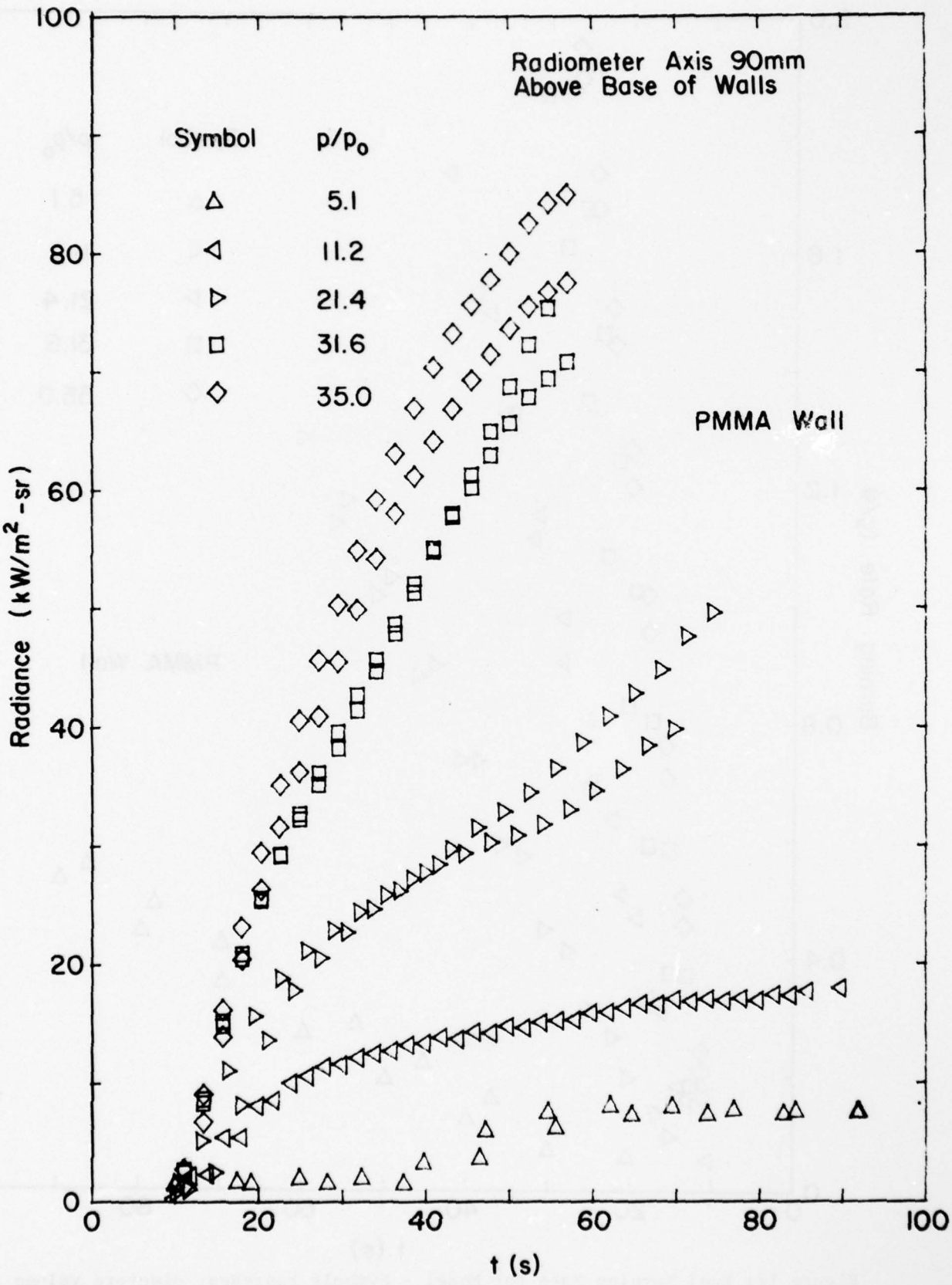

Figure 11: Flame and Fuel Radiance for Model

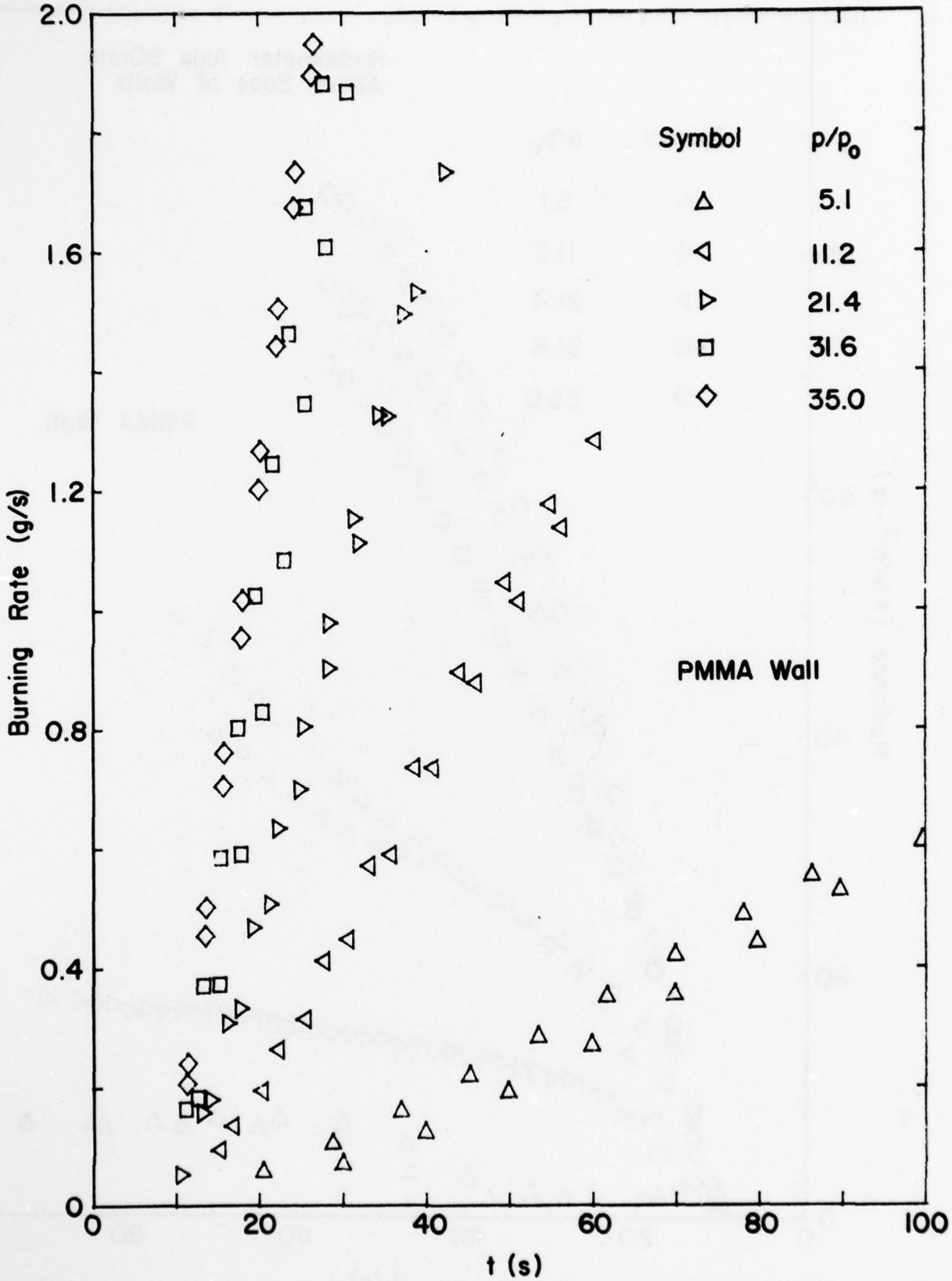

Figure 12: Fuel Burning Rate for Model - Symbols represent discrete values that are calculated from a least squares, fourth order polynomial fit to weight-loss data. Peak burning rates are only accurate to $\pm$ 1.0 g/test time.

MODELING VALIDITY

The preceding experimental data should be compatible with the pressure modeling scheme by which characteristic lengths are reduced as $p^{-2/3}$ and characteristic times as $p^{-4/3}$. With this scheme, pyrolysis height, flame height and maximum pyrolysis width are replotted in Figures 13, 14 and 15. It is clear that the great differences in the magnitude of the variables between the model and full-scale experiments is substantially reduced by the coordinates used in these figures.

As before, the absolute value of "t" for all the elevated pressure tests in Figures 13-15 is adjusted such that $x_p\ (p/p_o)^{2/3} \simeq 0.2$m at $t(p/p_o)^{4/3} \simeq 65$s, since 0.2m and 65s are the initial pyrolysis height and time measurements at one atmosphere. The pressure corrected data for the model and full-scale tests shown in Figure 13 are thus forced to be in good agreement just after initiation of flame spread on the prototype PMMA wall. This procedure is used since the time origin is always somewhat arbitrary and also because the ignition process itself is not being pressure modeled in this study.

The modeling technique appears from Figure 13 to be valid for the prediction of pyrolysis height for more than 1000 seconds subsequent to initiation of flame spread. Modeling success seems to be best in Figure 13 at the highest ambient pressures. Figure 14 shows that modeling of flame height is not quite as successful as the modeling of pyrolysis height. The transient behavior of flame height, however, is predicted very well, especially (as before) by the model tests at the highest ambient pressures. In Figure 15, it can be seen that the maximum width of the pyrolysis region is not modeled very accurately during the upward fire spread process. The width of the full-scale pyrolysis zone is apparently increasing with time at a much lower rate than is predicted by the elevated pressure experiments. However, pressure modeling does correctly show that the lateral extent of fire spread is far less than the vertical spread component. Furthermore, the lateral spread process is initially quite sensitive to the exact ignition mode and at later times may be greatly affected by the exact fluid mechanical boundary conditions. Differences between the model and prototype results for W_{pm} may therefore be due to the obvious differences in the ignition mode and to uncontrolled differences in flow boundaries near the experiments.

Because the pressure modeling scheme preserves the dimensionless groups (such as Grashof number) controlling the convective flow field, the convective Nusselt Number, or the product of length scale and heat transfer coefficient will be invariant. The reduction of all length scales as $p^{-2/3}$ in the model then means that convective heat fluxes must increase as $p^{2/3}$. All other heat fluxes, including flame radiance, should increase as $p^{2/3}$ to insure modeling success. This pressure correction is applied to the transient radiance measurements, with the result as shown in Figure 16.

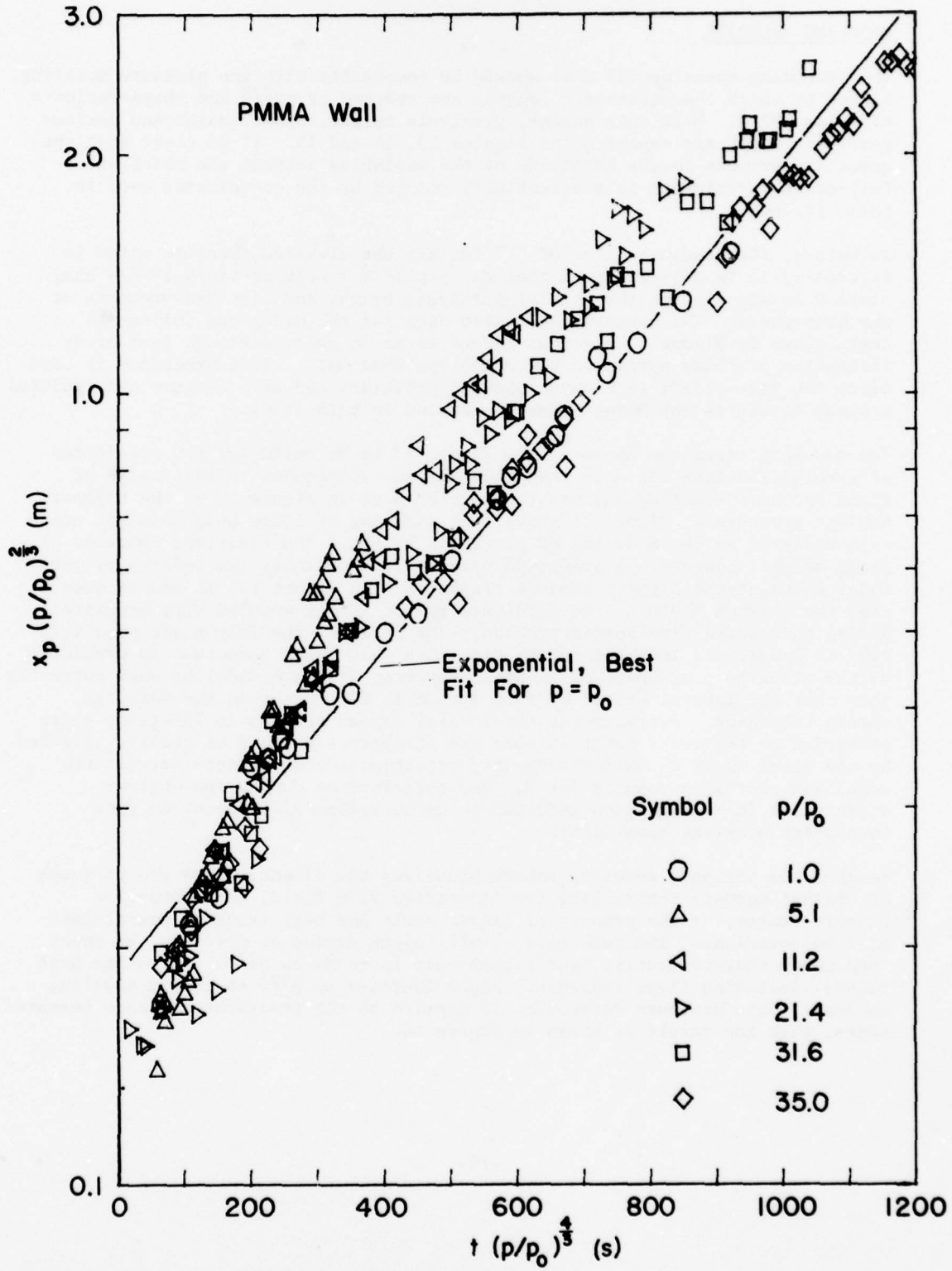

Figure 13: Correlation of Pyrolysis Zone Height

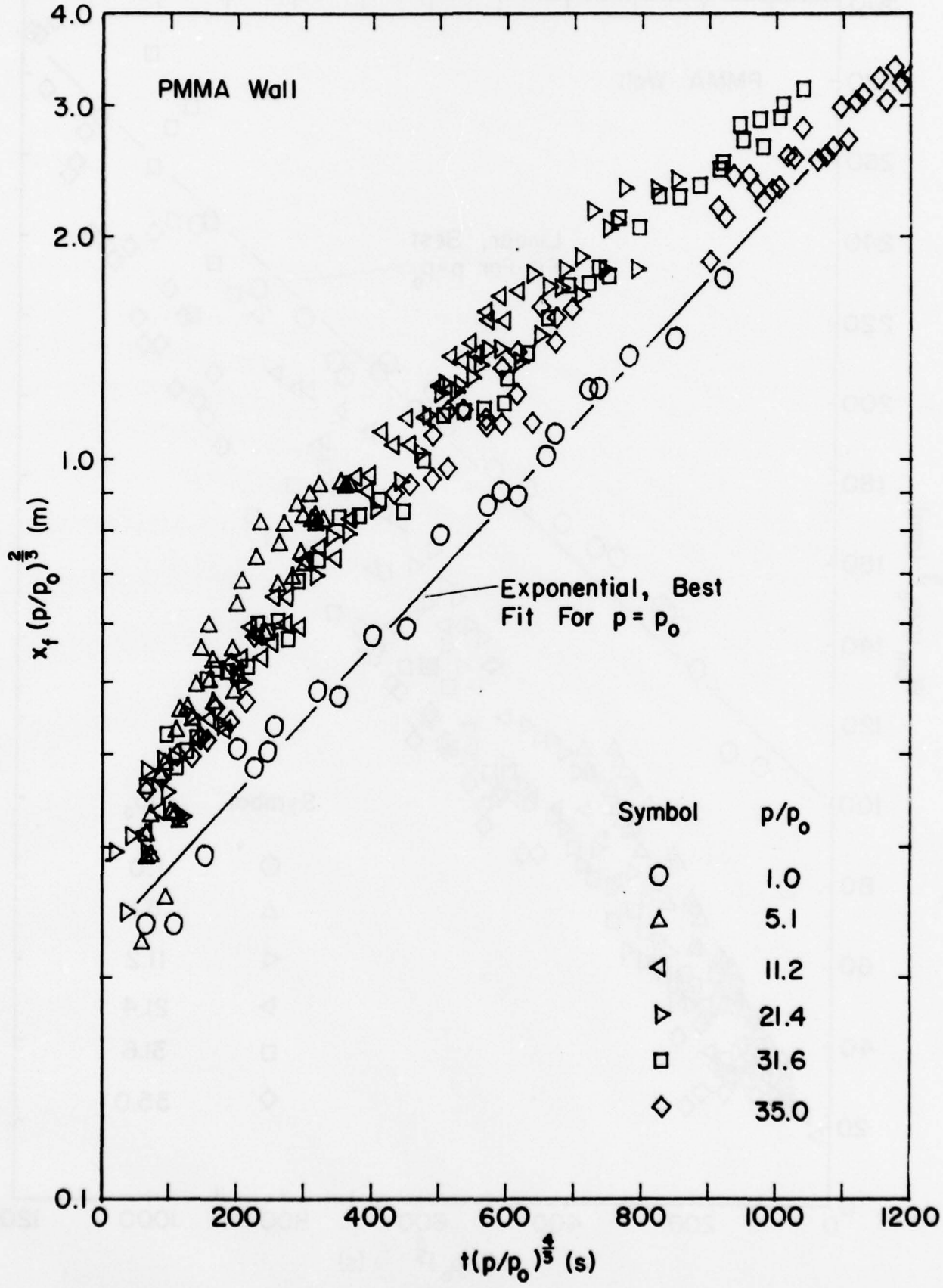

Figure 14: Correlation of Flame Height

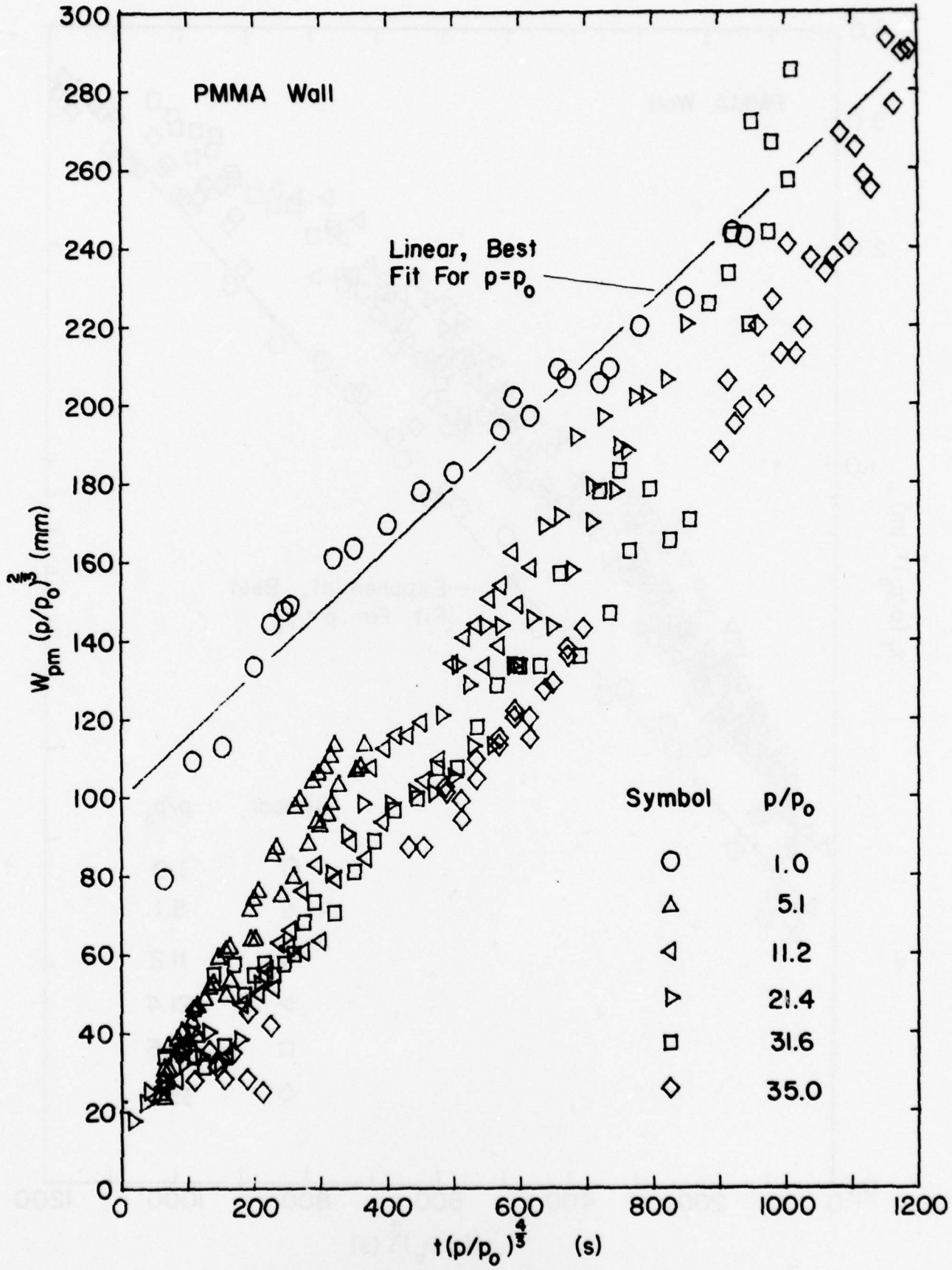

Figure 15: Correlation of Maximum Width of Pyrolysis Zone

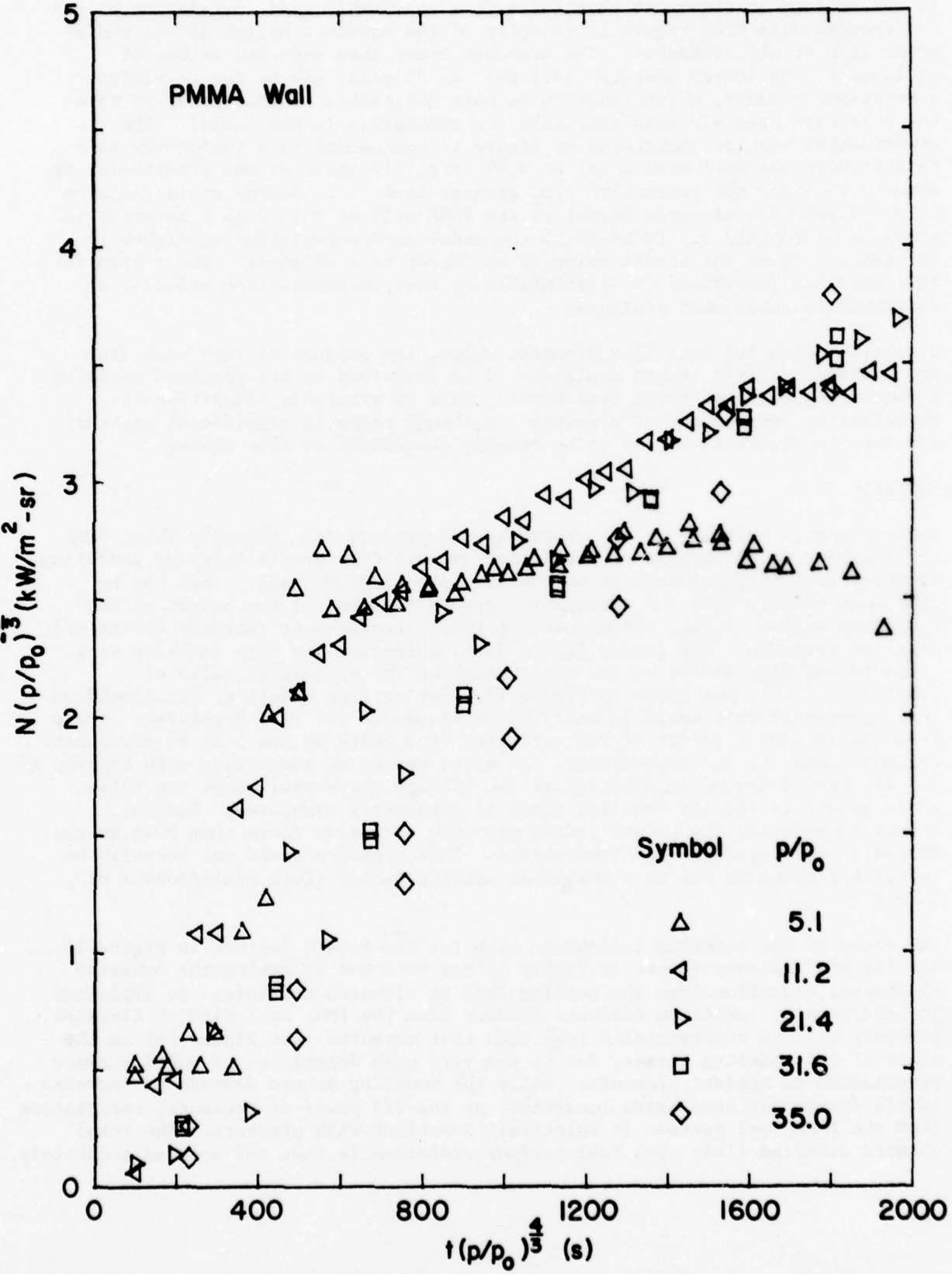

Figure 16: Correlation of Radiance Measurements for Model

It can be seen in Figure 16 that there is a reasonably good correlation of the uncorrected data from Figure 11 in spite of the constant height of the radiometer axis at all pressures. The somewhat lower than expected values of radiance at the lowest pressure (0.5 MPa, or 75 psia) may be due to radiant absorption by smoke, which tends to be more noticeable at this pressure when there is much less air mass available for combustion in the vessel. The experimental results correlated in Figure 16 correspond to a radiometer axis height above the wall base equal to 0.09 $(p/p_o)^{2/3}$ meter at one atmosphere, or about 0.75 m for the tests with p/p_o greater than 5.1. Steady state radiance at one atmosphere measured normal to the PMMA wall at this 0.75 m location is shown to be roughly 3.5 kW/m^2-sr by the model data correlation in Figure 16. Reference 4 shows the actual value to be closer to 6 kW/m^2-sr. The reason for this modeling inaccuracy is attributable to surface reradiation effects, as discussed in subsequent sections.

By analogy with the heat flux argument above, the product of fuel mass flux and a characteristic length scale should be preserved by the pressure modeling scheme. The ratio of total fuel burning rate to pyrolysis height should therefore be independent of pressure. Although there is significant scatter, the data in Figure 17 appear to be roughly correlated by this scheme.

ANALYSIS

While pressure modeling of the upward spread process for thermally thick PMMA walls appear to be capable of predicting overall fire growth behavior, modeling accuracy is strongly dependent on the absolute pressure used. This can be seen most clearly with the exponential growth factors for the height of the pyrolysis region, V_p/x_p, which modeling theory requires to increase as the 4/3 power of pressure. The growth factor data, corrected for this increase with pressure and also scaled by the one-atmosphere (or prototype) value of 2.408×10^{-3} s^{-1}, are shown in Figure 18. For perfect modeling, the dimensionless, corrected data would be unity in magnitude at all test pressures. There is actually over a factor of two variation from unity in the 5 to 40 atmosphere pressure range of the experiments. As noted before in connection with Figures 13 and 14, best modeling is achieved at the highest pressures, where the full-scale growth factor (or doubling time) is accurately simulated. However, errors in modeling the growth factor are only excessive (more than 50%) at the unusually low pressure of 5 atmospheres. This pressure would not normally be useful for modeling due to a resultant scaling factor (full scale/model) of only 2.9.

The cause of the modeling inaccuracy both for the growth factors in Figure 18 and for the radiance values in Figure 16 may be found by noting the behavior of thermal radiation from the burning PMMA at elevated pressure. As explained in reference 2, radiation directed outward from the PMMA wall fire at elevated pressure will be substantially less than that expected (see Figure 16) on the basis of the modeling scheme, due to the very weak dependence of solid surface reradiation on ambient pressure. While the modeling scheme demands an increase in all fluxes (at homologous locations) as the 2/3 power of pressure, reradiation from the PMMA fuel surface is relatively invariant with pressure. The total outward directed flame plus fuel surface radiation is thus not modeled accurately.

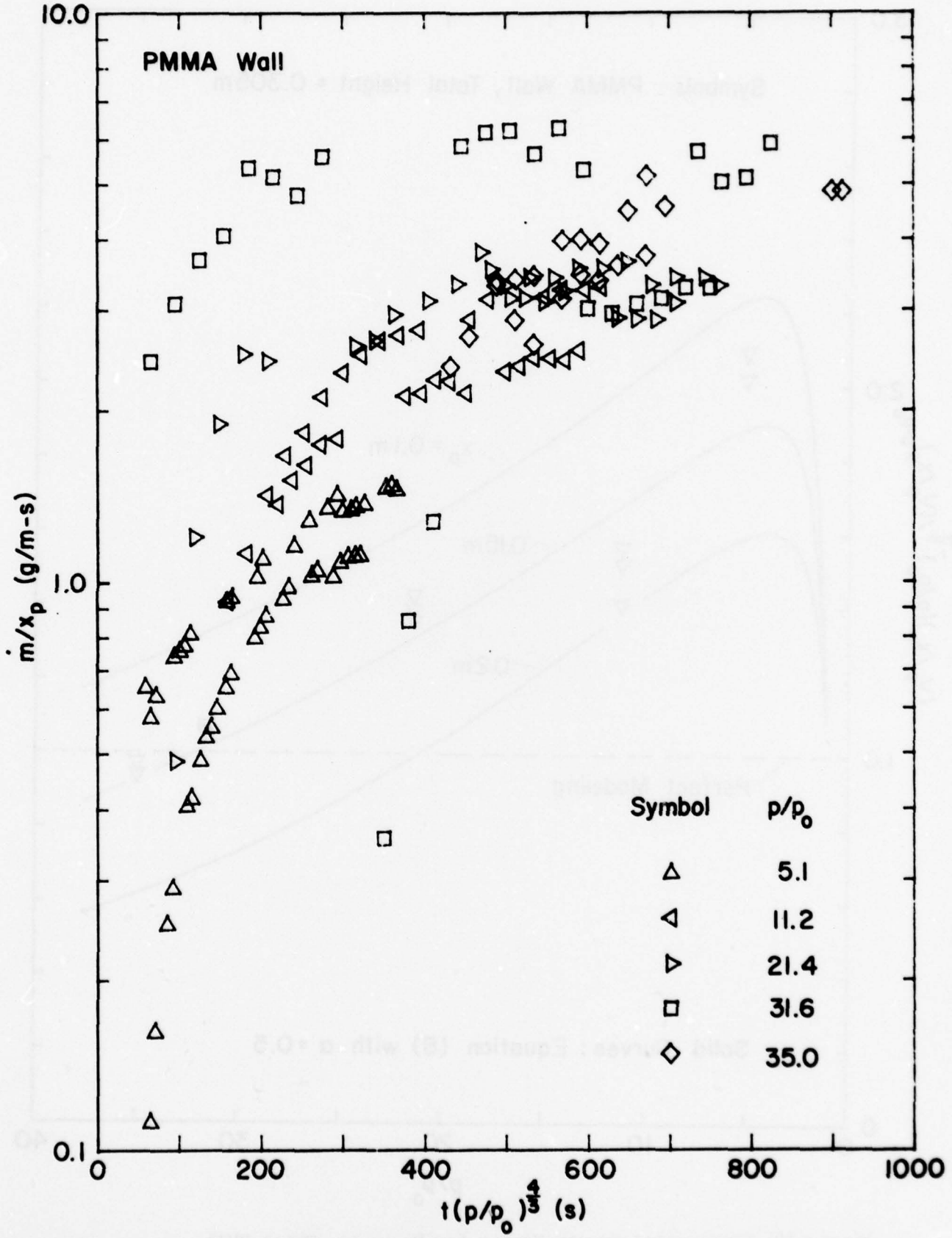

Figure 17: Correlation of Burning Rates for Model - Symbols are obtained from the discrete, calculated values of burning rate given in Figure 12.

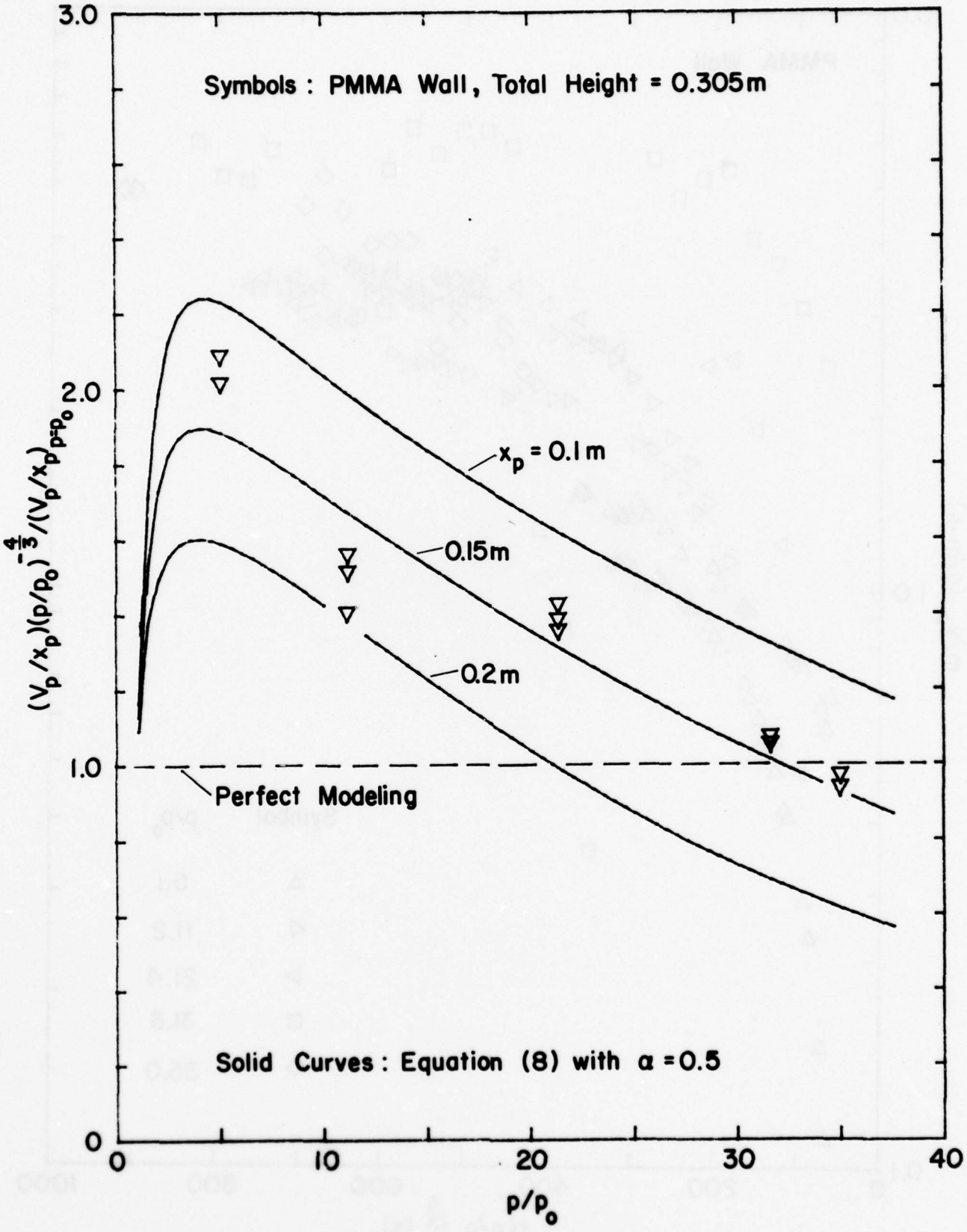

Figure 18: Exponential Growth Factor for Thermally Thick PMMA

It is shown in reference 2 that the flame radiation alone does increase sufficiently with pressure to be modeled adequately for a wide range of pressures. The constant surface reradiation, in fact, becomes negligible compared to the ever increasing flame radiation at elevated pressure. Because the pressure-corrected radiance data in Figure 16 therefore represents mainly contributions from the flame and not from the fuel surface, the model results in this figure should be compared with the flame radiance alone at full-scale. The steady-state flame radiance alone for a ray normal to the PMMA wall can be inferred to be 3.5 kW/m^2-sr from separate measurements of total radiance and surface reradiation in reference 4 (6 kW/m^2-sr and 8.6 kW/m^2, respectively) and from a calculation of flame transmittance (0.92) in reference 8. This value is in very good agreement with the model predictions in Figure 16.

The relative insignificance of surface reradiation loss at elevated pressure compared to flame radiative feedback results in a larger than required net radiative gain by the fuel surface as long as flame radiation increases sufficiently with pressure. This increased net heat flux to the fuel, beyond that expected for proper modeling, leads to the acceleration (see Figure 18) of the fire spread for moderate pressures. At higher pressures, flames become saturated (optically thick) and thus behave more like solid surfaces than like gaseous radiators. The flame radiant flux then does not increase with pressure as rapidly as demanded by the modeling scheme, leading to somewhat smaller rates of fire spread than expected (see Figure 18).

The preceding effects can be quantified to a great extent by utilizing approximate theoretical models of upward flame spread developed in references 4 and 9. These models show that the upward spread velocity, V_p, of the pyrolysis front on a thermally thick vertical wall is proportional to the pyrolysis height, x_p, and to the square of the net heat flux, $\dot{q}''$, to the fuel from the flame between the pyrolysis point, x_p, and the flame tip, x_f. Such an expression for spread velocity is compatible with the current study's observed fire spread behavior at all pressures, given by equation (1).

The model of flame spread developed in reference 4, unlike that in reference 9, is applicable when thermal radiation is an important or dominant mode of heat transfer, as in the case of upward fire spread on large-scale walls. For thermally thick walls, reference 4 gives the following model for spread velocity:

$$V_p = C x_p \dot{q}''^2 \, \ell n(x_f/x_p)/(T_p - T_\infty)^2 \qquad (2)$$

where C is a constant for a given fuel, T_p is the fuel pyrolysis temperature and T_∞ the ambient temperature.

The net heat flux to the unburnt fuel due to the upward spreading flame, $\dot{q}''$, can be evaluated from the following expression:

$$\dot{q}'' = \dot{q}''_f - \dot{q}''_{rr} + \dot{q}''_c \qquad (3)$$

where $\dot{q}''_f$ is the radiant flux from the flames, $\dot{q}''_{rr}$ is the reradiant loss from the heated but unburned fuel surface and $\dot{q}''_c$ is the convective heat flux to the fuel from the flames. Each of the terms in equation (3) is discussed in reference 8 for the case of a steadily burning, PMMA wall fire. With the assumption that the instantaneous heat transfer conditions to the unburned fuel above the point x_p are similar to those during steady fuel pyrolysis (with an exception noted below), the three heat flux terms in equation (3) become the following three terms:

$$\dot{q}'' = \sigma T_g^4 \left[1-\exp(-kL_m)\right] - 0.93\sigma T_p^4 \alpha + 5.5 \left(p/p_o\right)^{2/3} \qquad (4)$$

where $\dot{q}''$ is in $[kW/m^2]$, σ is the Stefan-Boltzmann constant, T_g the effective radiation temperature of the flame gases, k the flame radiation absorption coefficient, L_m the radiation mean-beam-length of the flame gas slab in front of the wall, and α is a reradiation constant between zero and unity.

The value of the mean-beam-length in the first term (flame heat flux) of equation (4) is given in reference 10 as 3.5 times the volume of the flame gases divided by the bounding surface area of the gases. For the present case, L_m is approximately $3.5\ W_f d/(2W_f+2d)$, where d is the thickness of the flame zone above x_p and W_f is the width of this zone. Since the point ignition leads to a very narrow flame zone above the pyrolysis point, it will be assumed that $W_f \simeq d$ and that therefore, $L_m \simeq 0.875d$. Measurements in reference 8, confirmed by calculations in reference 11, show that flame thickness, d, increases nearly linearly with height, x, such that $d = x/16$.

The reradiant heat loss during upward spread, represented by the second term in equation (4), is identical to that during steady burning except for the constant, α $(0<\alpha<1)$. This factor accounts for the temperature of the unburned fuel (above the pyrolysis point but below the spreading flame tip) being somewhere between T_p and T_∞. A value of 0.5 for α would seem reasonable. The magnitude of T_p is determined from a zero-order Arrhenius law for fuel pyrolysis, given in reference 3 for the case of steady burning, as follows:

$$T_{po}/T_p = 1 - (T_{po}R/E)\ \ln\ (\dot{m}''/\dot{m}''_o) \qquad (5)$$

where T_{po} and $\dot{m}''_o$ are the fuel pyrolysis temperature and mass flux, respectively, referenced to conditions at a PMMA wall height of 0.76 m and a pressure of one atmosphere, R is the universal gas constant, 8.31 J/mole-K and E is the Arrhenius activation energy of 1.257×10^5 J/mole. At the above reference conditions, the pyrolysis temperature, T_{po}, is 636 K (see reference 3) and the reradiant flux equal to $8.6\ \alpha\ kW/m^2$ since the fuel surface emissivity is about 0.93. For other than the reference conditions, the mass flux ratio, $\dot{m}''/\dot{m}''_o$, must be evaluated. Pressure modeling requires the fuel mass flux at homologous locations in the model and prototype to vary as $p^{2/3}$. This variation with pressure is more significant, in the present case, than the variation of $\dot{m}''$ with vertical position on the wall. As a result, $\dot{m}''/\dot{m}''_o$ in equation (5) can be replaced by $(p/p_o)^{2/3}$.

As discussed in reference 8, the flame convective heat flux to the PMMA fuel has been found to be nearly independent of vertical position and equal to about 5.5 kW/m^2 at 1 atmosphere. It is assumed here that this flux is accurately pressure modeled, leading to the 2/3 power dependence shown in the last term of equation 4.

Evaluation of the flame radiation properties, T_g and k, in equation (4) requires information to be obtained at elevated pressures as well as at one atmosphere. The effect of elevated pressures on the radiation properties of steadily burning PMMA wall fires has been the subject of a concurrent study by the author. Results of this study, to be reported in reference 6, show that at 10 atmospheres (1.0 MPa, or 165 psia) the effective radiation temperature, T_g, is nearly identical to the value of 1400K determined in reference 12 for one atmosphere conditions. Furthermore, the surface radiation term in equation 4 (with $\alpha = 1$ since the fire is steady) is found to be quite accurate at the 10 atmosphere pressure of the study. As expected, the flame absorption coefficient is found in reference 6 to increase significantly with pressure from the one-atmosphere value of 1.3 m^{-1} given in reference 12. Based on the magnitude measured at 10 atmospheres, k increases roughly as the 4/3 power of pressure. This dependence on pressure is precisely that required for accurate modeling of radiant flux from optically thin flames, for which $\exp(-kL_m) \simeq 1-kL_m$, and for which flame radiative flux is therefore given by $\sigma T_g^4 kL_m$, a quantity increasing as the required $p^{2/3}$. In addition, the assumptions that $T_g \approx 1400K$ independent of pressure and that $k = 1.3(p/p_o)^{4/3}\ m^{-1}$ are found to be generally consistent with the final, steady values of the radiance measurements shown in Figure 16.

It is assumed that the dependence of k on pressure determined in reference 6 extends to pressures above 10 atmospheres. If this assumption and the others discussed above are used in equation (4), the following expression for net heat flux to the unburned PMMA is obtained:

$$\dot{q}'' = \sigma(1400)^4[1-\exp(-0.071(p/p_o)^{4/3}x_p)]-8.6\alpha\left[1-0.042\ell n\,(p/p_o)^{2/3}\right]^{-4} + 5.5(p/p_o)^{2/3} \qquad (6)$$

where flame thickness, d, is taken to be $x_p/16$, and all flame properties are assumed to be uniform between the pyrolysis front and the flame tip.

Equation (2) shows that V_p depends not only on the net heat flux and the fuel pyrolysis temperature given by equations (5) and (6), but also on the ratio, x_f/x_p, of flame height to pyrolysis height. This ratio can be obtained from the exponential, least squares fits to the data in Figures 4-6. These expressions yield x_f/x_p proportional to x_p^{-n}, where n is typically from 0.17 to 0.11 for twelve elevated pressure experiments and about 0.03 for the single prototype experiment. A value of 0.11 is selected for "n" as a compromise.

As a result, the ratio of flame height to pyrolysis height becomes:

$$x_f/x_p = 1.3\ x_p^{-0.11} \tag{7}$$

where x_p is in [m].

The dimensionless growth factor expression used for plotting data in Figure 18 can now be obtained from equations (2) and (5) through (7) in the following functional form:

$$\frac{(V_p/x_p)(p/p_o)^{-4/3}}{(V_p/x_p)_{p=p_o}} = f\ (p/p_o, \alpha, x_p) \tag{8}$$

In evaluating equation (8), a pyrolysis height, x_p, at elevated pressure, p, is first selected for the 0.3 m high model walls. The equivalent quantity at $p=p_o$ is then computed as $x_p\ (p/p_o)^{2/3}$, which is the homologous location for the prototype.

Figure 18 contains a plot of equation (8) for three different values of x_p at elevated pressure. It can be seen that the variation of the dimensionless growth factor from the unity value expected for perfect modeling is explained quite well by the preceding analysis. Best agreement between theory and experiment is obtained when $\alpha = 0.5$ (as suggested in reference 4) and x_p = 0.15 m, the mid-height of the model walls.

The theoretical analysis thus appears to reinforce the conclusion, previously based only on the experimental data, that pressure modeling of upward fire spread on PMMA fuel is most practical and accurate for p/p_o ranging from 20 to 40.

APPLICATION OF MODELING TO AIRCRAFT MATERIAL FIRES

MODELING TECHNIQUE

In this study, samples of 15 different aircraft cabin materials provided by NAFEC are exposed to a point ignition source at elevated absolute air pressures of 1.1, 2.1 and 3.1 MPa (11, 21 and 31 atm or 165, 315 and 465 psia). To evaluate the hazard of upward fire spread, the NAFEC samples represent a wide variety of full-scale construction from uniform solids to foams, and from composites to textiles. Unless these samples are thermally thick at one atmosphere, the absolute magnitude of the sample thickness will in principle have some effect on the process of fire spread. A reduction in the thickness dimension at elevated pressure as $p^{-2/3}$ would then ordinarily be required to enable predictions of full-scale behavior to be made with the pressure modeling technique. Such thickness reductions are not always practiced, as in the present study.

The extrapolation to one-atmosphere conditions from elevated pressure experiments for materials of fixed physical thickness is facilitated by understanding the effect of pressure on the thermal wave thickness. This wave, representing the region of temperature rise in the fuel due to heat transfer from the spreading fire, becomes thinner as ambient air pressure is increased due to the increase in heat flux and surface regression rate with pressure. As a result, materials of fixed size which are thermally thick (physical thickness of material much greater than thermal wave thickness) at one atmosphere will remain thermally thick at elevated pressures. The same procedure used before with the PMMA walls can be repeated with such thermally thick materials in order to obtain one-atmosphere spread rates from measurements with a model at elevated pressure (spread rates increase as $p^{2/3}$).

On the other hand, materials of fixed size which are thermally thin (negligible internal temperature gradients) at one atmosphere must eventually become thermally thick at a sufficiently high ambient pressure as the thermal wave thickness decreases. The material may, however, remain thermally thin up to some maximum ambient pressure, beyond which the change to a thermally thick behavior occurs. It is shown in references 1 and 4 that for such thermally thin behavior up to some maximum pressure, upward spread velocity at homologous locations should be independent of pressure if the physical thickness of the material remains constant. Spread rates at a full-scale vertical position at one-atmosphere in this instance could be obtained from measurements with a model of full-scale physical thickness, at elevated pressures, as long as thermally thin behavior is preserved.

EXPERIMENTAL ARRANGEMENT

In this application of pressure modeling, small-scale samples of the real aircraft materials provided by NAFEC are used. Rates of vertical flame spread at elevated pressure are measured in order to predict the performance of the materials at full-scale. Experimental conditions are similar to those of the PMMA model tests, with exceptions described below.

The NAFEC materials used in this flame spread study are identical in size (70 mm x 305 mm high) with samples employed in the FAA one-atmosphere vertical Bunsen burner test. The FAA test is a modification of Federal Test Method No. 191, in which a Bunsen flame is applied to the lower edge of a vertical fabric sample to initiate upward flame spread. A similar test has been proposed recently in reference 13. As shown in the schematic in Figure 19, the NAFEC materials for the present study are positioned vertically on a load platform in a clamp-type fuel holder which leaves a 50.8 mm sample width and the full sample height exposed. It is found that the steel holder effectively confines flame spread to the exposed 50.8 mm width. Flame spread can occur on the back side of the samples once flame on the front side burns through the materials since no insulation or other backing is used with the sample holder. Such back-side flame-spread does not occur because of the PMMA igniter piercing the sample.

The NAFEC samples are exposed to an ignition source at a single small point about 25.4 mm above the bottom edge of the material (see Figure 19), in keeping with the general ignition mode for the model PMMA walls (see Figure 1). However, the toothpick ignition source used for PMMA has insufficient energy to ignite several of the NAFEC materials, as shown in the results section below. A 6.35 mm diameter PMMA rod extending out beyond the fuel surface 50.8 mm is found to be satisfactory in this case for initiating fire spread over all but one of the fifteen materials. Both the toothpick and PMMA rod have a reasonably uniform, reproducible composition and burn with negligible residue. The PMMA rod used is produced by casting, rather than by extrusion, to avoid any dripping of the liquid monomer while a flame propagates down the rod from the paper wick igniter. Cast rods of smaller than 6.35 mm diameter are not readily available. Further details of the ignition scheme are illustrated in Figure 19, where it is shown that the ignition rod passes through a tight-fit hole in the sample but is supported by the aluminum angle behind the sample.

The aircraft cabin materials used in this study, identified by NAFEC sample numbers placed on the back (away from the aircraft interior) sides, are prepared by being placed in an environmental chamber for several days prior to each experiment. Temperature and relative humidity are controlled at 21 deg. C and 40%, respectively, in the chamber. Samples are then removed to the pressure vessel in plastic bags for mounting in the fuel holder shown in Figure 19, with the front side of each sample exposed to the PMMA rod ignition source. Fabric samples are tested in only one orientation, such that any noticeable grain direction is horizontal. The relative humidity of the air supplied to the pressure vessel itself for each experiment is exceptionally dry for two reasons: 1) dual cartridge dryers on the air compressor outlet reduce the dewpoint of air at a pressure of 200 atm (20 MPa) to -53 deg. C and 2) the dried air is stored at 200 atm before being reduced in pressure to below 55 atm (5.5 MPa) for supply to the test vessel. The latter pressure reduction process insures that even if the cartridge dryers fail, the relative humidity of the air in the pressure vessel prior to ignition is no more than 20 to 30%. As shown

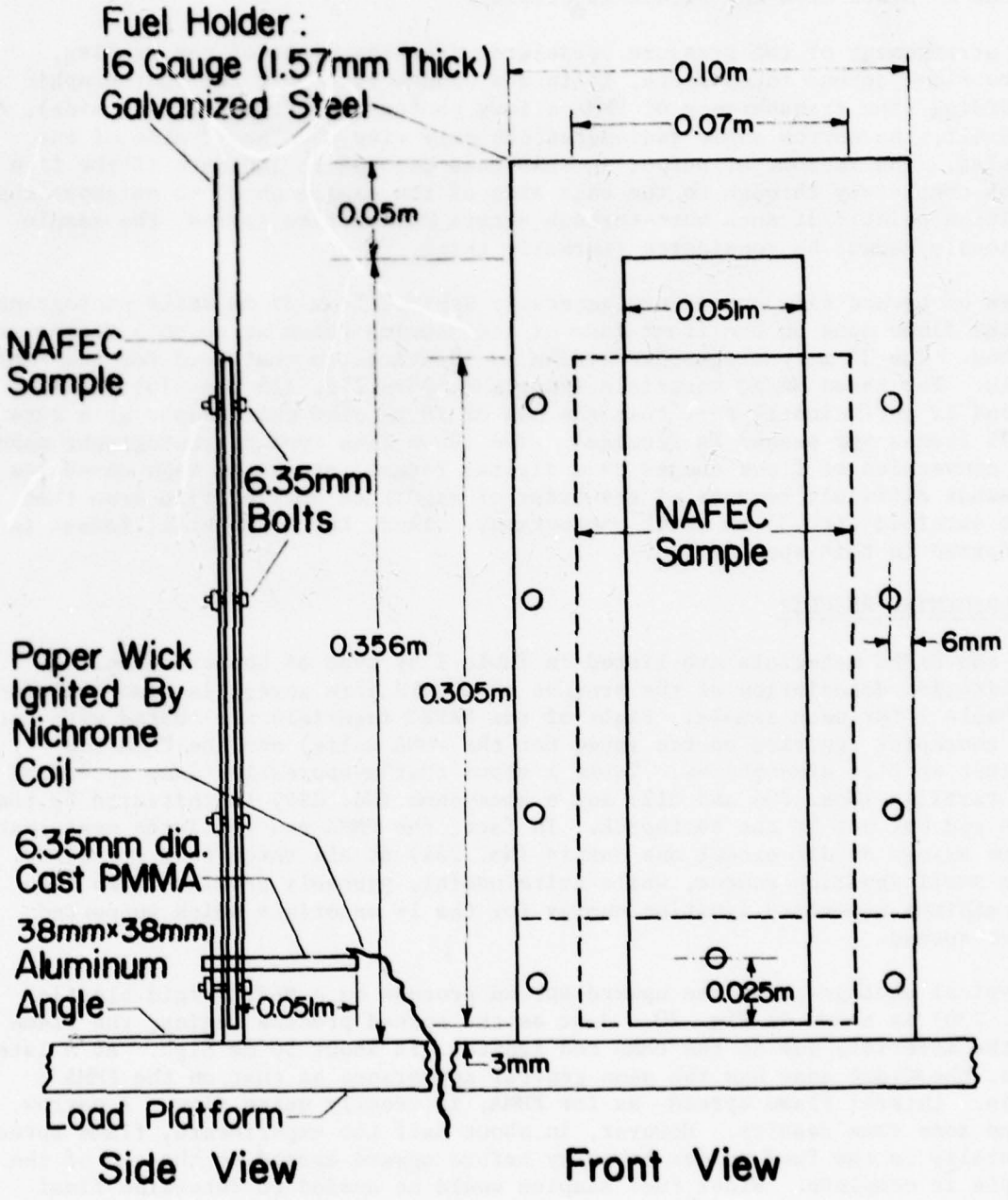

Figure 19: Schematic Diagram of Aircraft Cabin Material in Fuel Holder

in reference 3, the high pressure dry air in the test vessel rapidly removes excess moisture from any porous materials.

The arrangement of the pressure vessel requires the front of the samples, where flame spread takes place, to face a window view-port for photographic recording (the transparency of PMMA allows photography from the back side). As a result, the narrow angle radiometer can only view the "back" side of the samples. The radiometer output in this case is used to indicate if the fire burns completely through to the back side of the sample about 65 mm above the ignition point. If such burn-through occurs during fire spread, the sample obviously cannot be considered thermally thick.

Rates of upward fire spread are generally derived from 35 mm still photographs of the flame zone on the front face of the samples taken at up to 5 frames per second. The 35 mm photographic system is identical to that used for the PMMA walls. For three NAFEC materials (sample numbers 213, 215 and 226) flame spread is sufficiently fast that the use of 16 mm cine photography at a rate of 25 frames per second is required. The 16 mm cine type of photography makes the conversion of flame shapes to a digital format, stored on tape cassettes, somewhat difficult because of the order of magnitude smaller film area than that obtained with 35 mm still photography. Thus, the 35 mm still format is preferred in this application.

EXPERIMENTAL RESULTS

All the NAFEC materials are listed in Table 1 by type of construction. A qualitative description of the process of upward fire spread is also included in Table 1 for each sample. Eight of the NAFEC materials are tested with both the toothpick ignition source (used for the PMMA walls) and the PMMA rod ignitor at 21.4 atmospheres. Table 1 shows that measureable flame spread on two textiles (Nos. 204 and 212) and a honeycomb (No. 224) is initiated by the PMMA rod but not by the toothpick. In fact, the PMMA rod initiates measureable flame spread on all except one sample (No. 234) at all three test pressures. This small ignition source, while quite useful, probably provides more than the minimum necessary ignition energy for the 14 materials which supported flame spread.

A typical photograph of the upward spread process on a NAFEC rigid plastic (No. 230) is shown in Fig. 20. Just as the spread process begins, the flame on the material, due to the PMMA rod ignitor, is about 50 mm high. At a later time, the flame zone has the same general appearance as that on the PMMA walls. Lateral flame spread, as for PMMA, is usually quite slow. A narrow flame zone thus results. However, in about half the experiments, flame spreads laterally to the fuel holder boundary before upward spread to the top of the sample is complete. Wider fuel samples would be needed to determine final flame shapes in these cases. Another aspect of fire spread on the samples is the presence of thick smoke in most cases. This smoke obscures the flame tip and much of the upper portion of the flame zone in many photographs.

UPWARD SPREAD. During the process of flame spread on the samples, the rate of upward spread may drop sharply well before flame has progressed to the top edge (0.28 m above the ignition point). This sudden drop in spread rate usually leads to rapid flame self-extinguishment or incomplete upward flame spread. Table 2 lists those samples which exhibit this behavior. Such materials are maintained under pressure in the test vessel for several minutes after flames are no longer visible. Once the vessel is vented, the process of incomplete flame spread is clearly evident on the sample residue. In a few cases, noted in Table 2, a sudden drop in upward spread rate results in very slow flame propagation to the top edge instead of self-extinguishment.

From photographs such as those in Figure 20, two types of measurements are obtained for each NAFEC material ignited by the 6.35 mm dia. PMMA rod fire at absolute ambient pressures of 1.1, 2.1 and 3.1 MPa: 1) the average height, x_f, of the flame tip above the bottom edge of the sample and 2) the maximum width, W_{fm}, of the flame zone, which generally has a nearly uniform width for most of the flame height. These measurements are recorded as a function of test time, with t=0 generally several seconds before the actual ignition of the material. Typical plots of flame height, x_f, as a function of time are shown in Figure 21 for the case of complete flame spread to the top edge of four different NAFEC materials. In Figure 22, typical examples of x_f versus t behavior are shown for the case of incomplete flame spread, or flame self-extinguishment. It is evident that the flame height is growing exponentially with time (log x_f linear with t) during much of the upward spread process.

Both linear and exponential least squares fits to the data on flame height versus time have been tested for all 14 NAFEC materials that ignited. Such regression fits ignore flame height data when fire spread rates are close to zero, due to delayed ignition or incipient self-extinguishment. For more than 60% of all the spreading fires, regression (or correlation) coefficients are slightly higher with the exponential fit, a linear fit being slightly better for the remainder. An exponential fit also yields higher regression coefficients for more than half of those experiments in which self-extinguishment occurs. However, data from tests where a sudden drop in spread does not lead to self-extinguishment are fit somewhat better by a linear dependence of x_f on t. Examples of the best-fit exponential are shown in Figure 22 for tests where there is self-extinguishment of upward spread. Such fits are seen to give good results when there is sufficient duration of fire spread before extinguishment.

Exponential growth factors ("B" in equations (1) and (2)), V_f/x_f, applicable to each of the NAFEC materials are listed in Table 3 along with the corresponding regression coefficients. Since these coefficients are generally greater than 0.90 to 0.95, the exponential fit to the flame height data should be most useful for characterizing rates of upward spread on the aircraft materials, as is the case for the PMMA walls. Note that regression coefficients are generally lowest when fire spread is incomplete, due to insufficient data on flame heights.

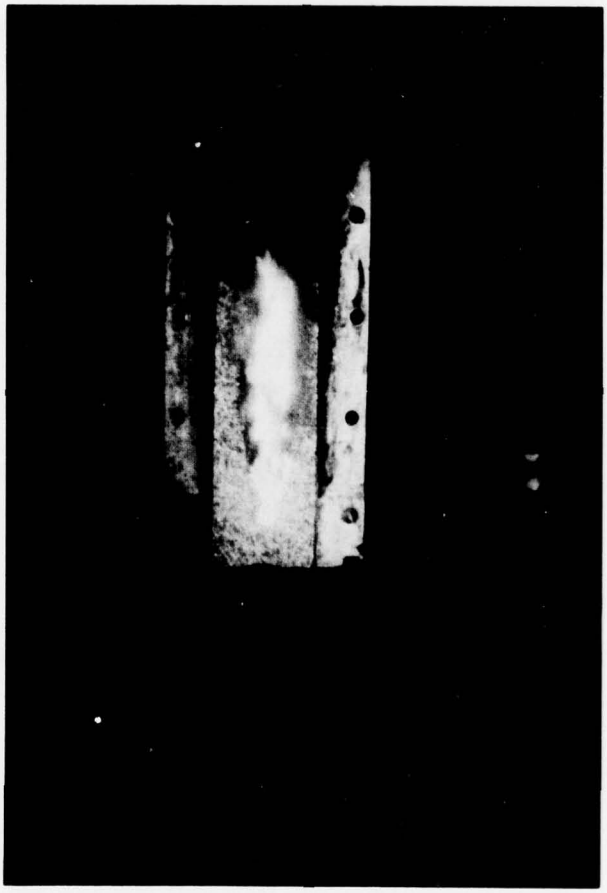

FIGURE 20. TYPICAL PHOTOGRAPH OF UPWARD FIRE SPREAD ON AIRCRAFT MATERIAL - NAFEC No. 230 AT p/p_o = 21.4

Table 1. Description of Aircraft Samples

NAFEC I.D. NUMBER	MATERIAL TYPE	IGNITION BEHAVIOR $p/p_o = 21.4$	COMMENT
204	Textile (Wool/Nylon, 90%/10%)	NT	
209	Textile (Treated Nylon)	P	Very slow upward spread with little visible flame.
210	Flexible Solid (Polyvinyl chloride)	T	Rapid ignition and spread.
212	Textile (Wool)	NT	
213	Foam (Polyurethane-33 kg/m^3)	T	Upward spread too rapid for visual observation.
215	Foam (Polyurethane-66 kg/m^3)	T	Same as #213
220	Rigid Solid (Polysulfone sheet)	P	No self-sustained flame spread at p/p_o = 11.2. Ignition generally delayed by appearance of a protruding char.
224	Honeycomb (Composite of polyvinyl fluoride/ fiberglass/phenolic/epoxy/ honeycomb of aromatic polyamide and phenolic with blocking of rigid polyurethane foam)	NT	Spread within honeycomb core as well as on surface.
225	Honeycomb (Composite similar to #224)	P	Limited spread, mainly on surface.
226	Textile (Wool carpet)	T	Flame spread mainly in carpet pile.
227	Honeycomb (Composite similar to #224 but without foam blocking).	P	Flame spread confined to surface layer.
230	Rigid Solid (Polyvinyl chloride/ABS)	P	At p/p_o = 21.4, upward spread is erratic, flame spread rate may drop temporarily.
233	Honeycomb (Composite of fiberglass/epoxy/ aromatic polyamide honeycomb/ polyvinyl fluoride)	P	Flame spread mainly on surface.
234	Rigid Solid (Polyester/fiberglass)	NT, NP	No self-sustained flame spread; some reinforcing fiber exposed for 0.04 m above ignition point.

Table 1. Description of Aircraft Samples (Cont.)

NAFEC I.D. NUMBER	MATERIAL TYPE	IGNITION BEHAVIOR $p/p_o = 21.4$	COMMENT
235	Rigid Solid (Polycarbonate)	P	

Key to Ignition Behavior:

NT - No ignition with toothpick
T - Ignition with either toothpick or with PMMA rod
NP - No ignition with PMMA rod
P - Ignition with PMMA rod - not tested with toothpick

Table 2. Aircraft Samples with Incomplete Upward Spread

$p/p_o = 11.2$

NAFEC I.D. NUMBER	COMMENT
204	Fire spread for a distance of 0.1 m above ignition point.
212	Fire spread for a distance of 0.08 m above ignition.
215	Fire spread for a distance of 0.08 m above ignition.
220	No self-sustained, upward spread.
225	Fire spread for a distance of 0.12 m above ignition.
227	Fire spread for a distance of 0.11 m above ignition.
230	Fire spread for a distance of 0.08 m above ignition.
233	Fire spread for a distance of 0.1 m above ignition.
234	No self-sustained, upward spread.

$p/p_o = 21.4$

NAFEC I.D. NUMBER	COMMENT
204	Spread incomplete in one test out of three.
209	Sharp drop in upward spread rate at x_f=0.1 m in two tests.
225	Spread a distance of 0.1 m above ignition-two tests.
230	Spread incomplete in one test out of two.
234	No self-sustained, upward spread.

$p/p_o = 31.6$

NAFEC I.D. NUMBER	COMMENT
234	No self-sustained, upward spread.

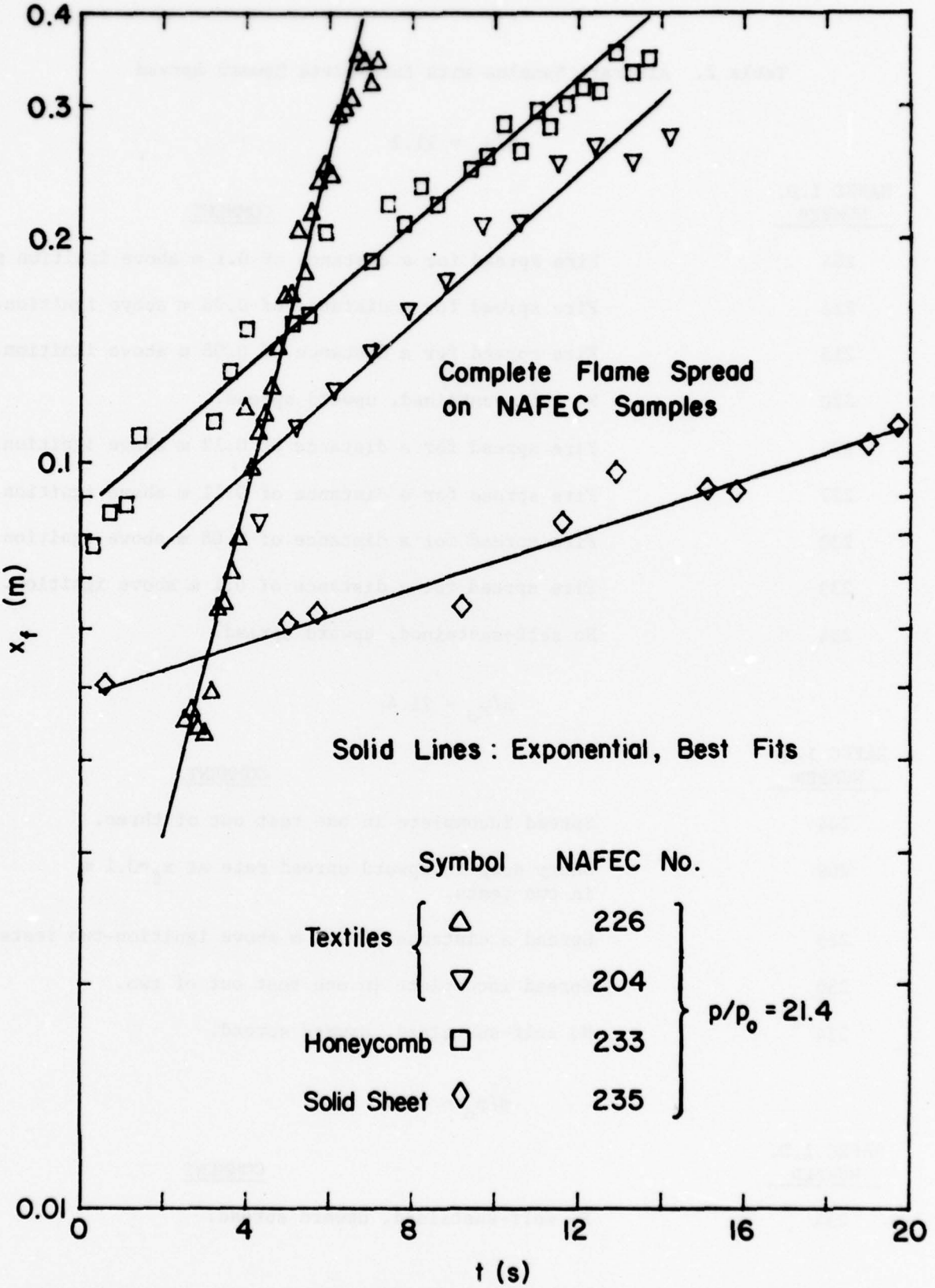

Figure 21: Examples of Flame Height for Complete Fire Spread - Data acquisition begins at t=0, which roughly coincides with ignition of the sample.

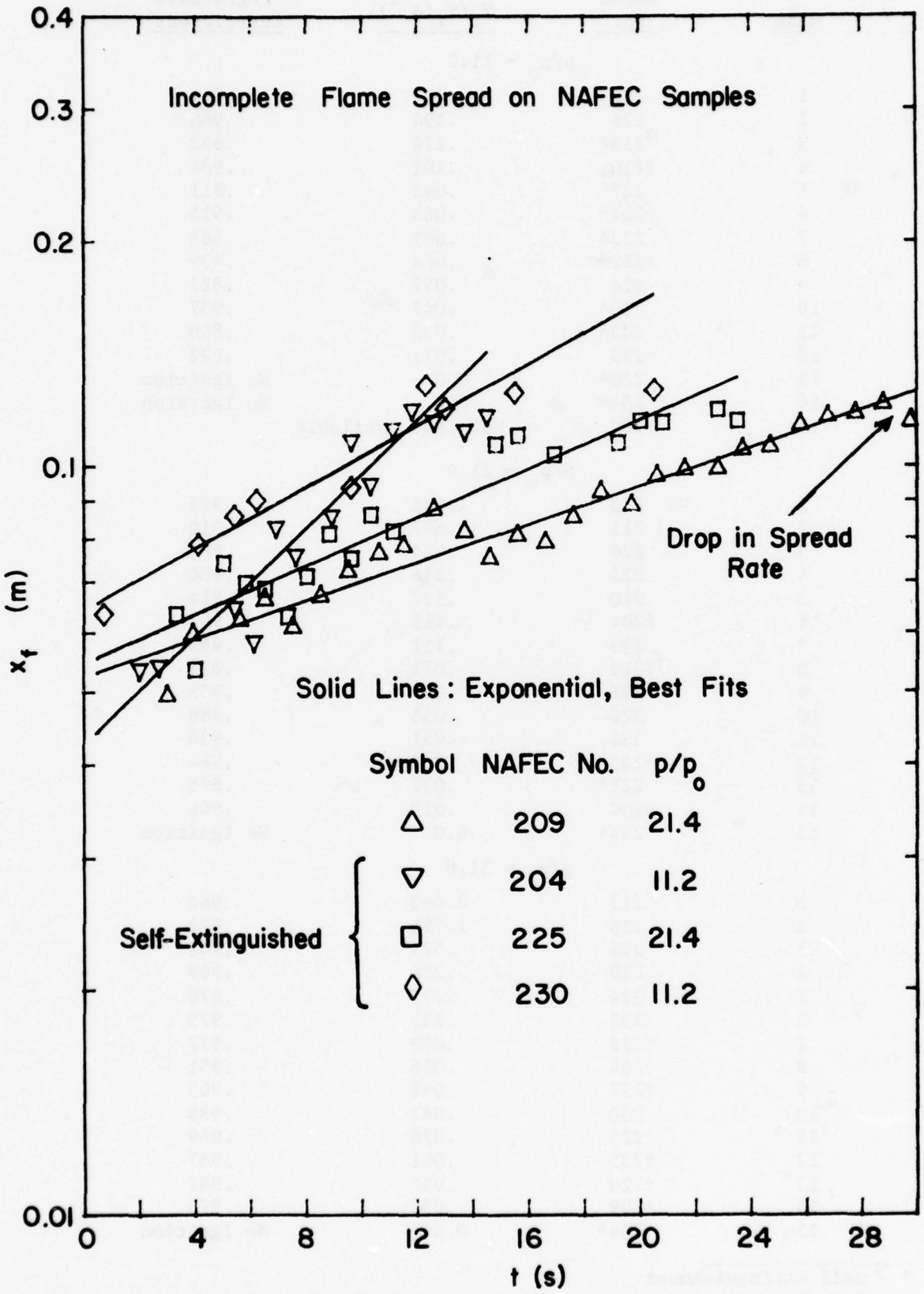

Figure 22: Examples of Flame Height for Incomplete Fire Spread - Data acquisition begins at t=0, which roughly coincides with ignition of the sample.

Table 3. Upward Spread Exponential Growth Factors for NAFEC Samples

Rank	NAFEC No.	$V_f/x_f(s^{-1})$	Regression Coefficient
		$p/p_o = 11.2$	
1	213	.417	.961
2	226	.194	.960
3	215*	.174	.852
4	†210	.101	.986
5	227*	.092	.811
6	†204*	.083	.915
7	233*	.081	.585
8	†212*	.062	.439
9	224	.057	.827
10	230*	.047	.937
11	225*	.033	.890
12	†235	.021	.992
13	220*	0.0	No Ignition
14	234*	0.0	No Ignition
15	†209	Data Not Available	
		$p/p_o = 21.4$	
1	213	1.404	.975
2	215	.897	.910
3	226	.524	.971
4	224	.216	.986
5	210	.132	.914
6	†204	.115	.943
7	233	.111	.968
8	†212	.071	.871
9	†227	.069	.955
10	220	.055	.988
11	230	.051	.936
12	†235	.042	.984
13	225*	.037	.895
14	†209	.029	.944
15	234*	0.0	No Ignition
		$p/p_o = 31.6$	
1	213	2.663	.962
2	215	1.781	.973
3	226	.571	.946
4	210	.286	.969
5	224	.273	.978
6	233	.157	.978
7	†212	.099	.977
8	†204	.095	.951
9	†227	.092	.963
10	230	.082	.985
11	225	.078	.969
12	†235	.061	.987
13	†220	.051	.982
14	†209	.032	.976
15	234*	0.0	No Ignition

* - Self Extinguishment
† - Burn Through

The growth factors listed in Table 3 are seen to vary by almost two orders of magnitude at each of the three ambient pressures. NAFEC materials are ranked in Table 3 according to the magnitude of these growth factors. The ranking, it should be noted, does not change significantly over the three-fold increase in ambient pressure of the tests. Furthermore, the ranking doesn't seem to be affected by the many occurrences of self-extinguishment at the two lowest pressures. This property of the spread process can be illustrated by one unusual case, NAFEC number 204 at 21.4 atm, for which fire spread is complete during a preliminary experiment but for which self-extinguishment occurs in the final run. Growth factors while upward spread is actually in progress are nearly identical for these two experiments.

During the upward spread process, all fuel may be consumed near the base of the sample, leading to flames on the back side before spread on the front side is either complete or self-extinguished. Such burn-through behavior, detected by the narrow angle radiometer (see previous section) and usually confirmed by inspection of the photographs, is indicated in Table 3. Three of the four textile materials (Nos. 204, 209 and 212) consistently exhibit this behavior, in addition to one rigid plastic (No. 235). Complete consumption of fuel at the base of the samples can result in shorter flames and hence less preheating of unburned fuel.

LATERAL SPREAD. Data on the nearly uniform width of the flame zone as a function of time are plotted in Figure 23 for a few representative NAFEC materials. In all cases, the width, W_{fm}, increases roughly linearly with time until just before flame spreads to the exposed width, W_o, of the sample. The lateral spread rate, $U_f = 1/2\ d\ W_{fm}/dt$, can, in effect, be considered a constant as the flame zone propagates a distance of about $W_o/2$. A characteristic spread time would therefore be W_o/U_f.

Table 4 contains an ordered list of the characteristic, lateral spread times for all the NAFEC materials. In addition, the times needed to double the flame height (ln2/growth factor) are shown, allowing the lateral and upward spread rates to be compared. It can be seen that the ranking of the NAFEC materials on the basis of lateral spread rate is very similar to that based on upward spread rate. NAFEC material number 209 is an obvious exception, having the lowest value of upward spread rate of all the samples but an intermediate lateral spread rate. This material represents the only case for which the lateral spread rate is far greater than the upward spread rate. Generally, the reverse is true, a not surprising result.

In spite of the small rates of lateral spread, the flame zone more often than not will reach the metal fuel holder at the sample side boundaries while the flame tip is still about 0.1 m from the top of the 0.3 m high sample. Such occurrences are indicated in Table 4 but do not appear to have any noticeable effect on rates of upward spread, For NAFEC material number 209, the flame tip is still more than 0.2 m from the top of the sample when the full exposed width of the material is involved.

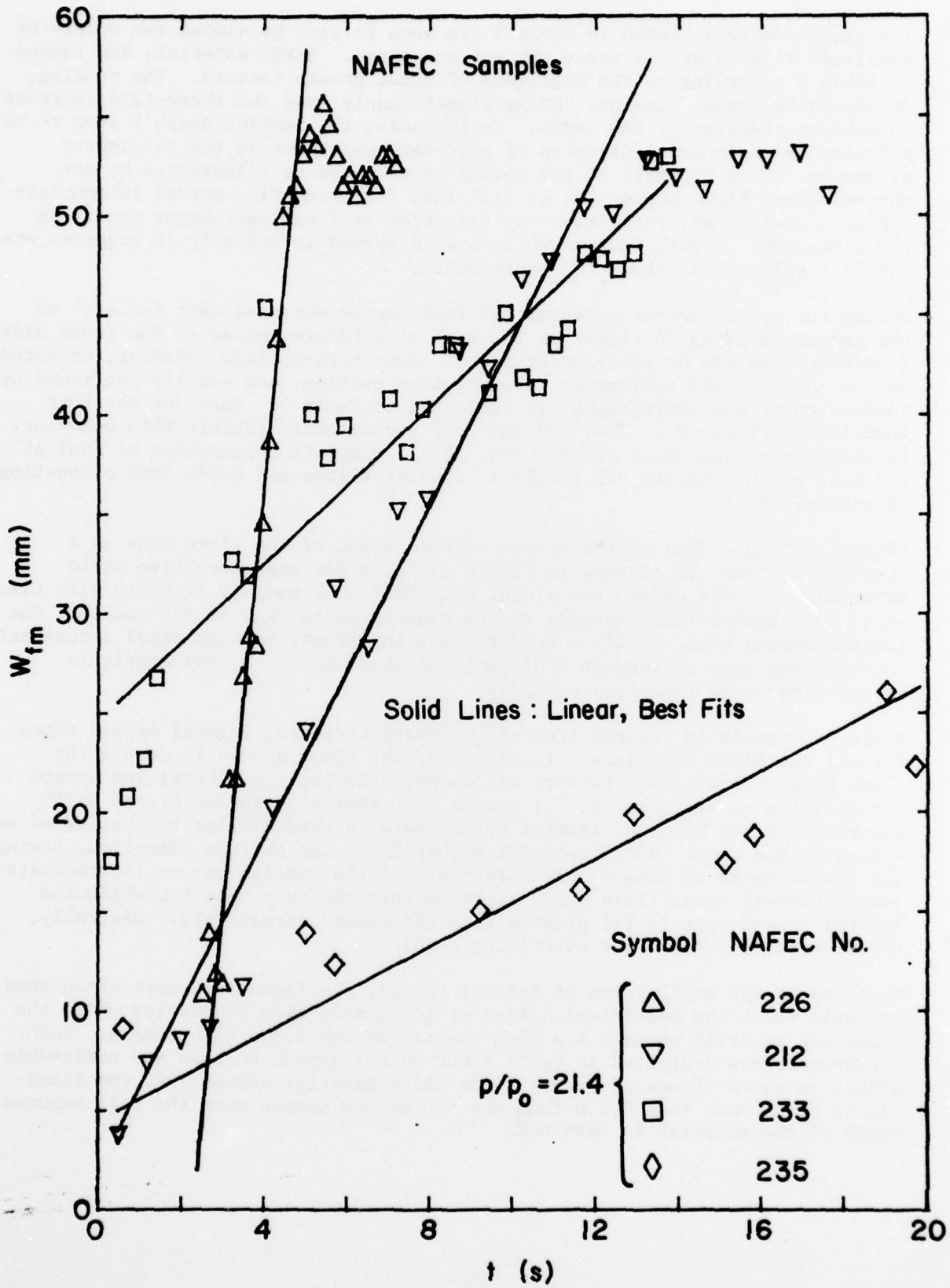

Figure 23: Examples of Maximum Flame Width - Data acquisition begins at t=0, which roughly coincides with ignition of the sample.

Table 4. Characteristic Times for Lateral and Upward Fire Spread: NAFEC Samples

Rank	NAFEC No.	Lateral Spread Time W_o/U_f(s)	Upward Spread Time $\ell n2/(V_f/x_f)$ (s)
		p/p_o = 11.2	
1	*213	2.474	1.661
2	215	4.869	3.976
3	*226	7.428	3.574
4	204	12.291	8.340
5	*210	15.516	6.860
6	212	21.998	11.091
7	233	27.863	8.524
8	227	31.275	7.510
9	230	39.205	14.612
10	224	50.470	12.063
11	225	83.861	21.138
12	*235	108.641	32.503
13	220	No Ignition	
14	234	No Ignition	
15	209	Data Not Available	
		p/p_o = 21.4	
1	*213	1.037	.494
2	*215	1.512	.773
3	*226	2.373	1.322
4	*204	6.684	6.011
5	224	9.130	3.215
6	*212	12.101	9.757
7	*210	12.366	5.270
8	*209	14.168	23.685
9	233	25.668	6.224
10	*220	36.063	12.685
11	227	41.814	10.085
12	225	43.214	18.527
13	*235	46.043	16.547
14	230	57.203	13.482
15	234	No Ignition	
		p/p_o = 31.6	
1	*213	.411	.260
2	*215	.900	.389
3	*226	1.799	1.215
4	210	5.620	2.420
5	224	7.155	2.539
6	*204	7.216	7.311
7	*209	8.255	21.921
8	*233	9.959	4.420
9	*212	10.759	7.032
10	*225	18.482	8.940
11	227	30.761	7.571
12	230	36.140	8.443
13	235	36.336	11.364
14	220	38.871	13.500
15	234	No Ignition	

* - Lateral spread to Fuel Holder before vertical spread is complete

MASS LOSS. The burning NAFEC samples are weighed continuously while fire spread is in progress. However, since fuel mass loss during fire spread is generally less than about 5 grams and sensitivity of the load measurement system is only $\pm$ 1 gram, calculated burning rates should be viewed as rough approximations to the actual values.

Typical data for materials with significant fuel mass loss are shown in Figure 24. A linear fit is seen to represent peak rates of mass loss adequately. The constant burning rates resulting from such linear fits are listed in Table 5, along with the regression coefficients. Ranking of the NAFEC materials by magnitude of burning rate in Table 5 is similar to the ranking based on upward or lateral spread rate in Tables 3 and 4. The burning rate ranking is also reasonably independent of ambient pressure.

ANALYSIS

The discussion in this section will be mainly concerned with the exponential growth factors for upward flame spread on the NAFEC samples. Measurements of lateral flame spread rates and mass loss rates are not nearly as reliable as the upward spread data because of the very small lateral extent of the flame and very small amount of fuel consumed, respectively. Use of somewhat wider samples and a more sensitive load transducer system would improve the accuracy and hence usefulness of the lateral spread and mass loss measurements.

As discussed before, a simple interpretation of measurements at elevated pressure depends on whether a material can be classified as thermally thin or thick during flame spread. One could assume that all of the materials are thermally thick during flame spread at high pressure due to decreased thermal wave thickness. With this assumption, extrapolation of the relative fire spread hazard from elevated pressure to one atmosphere would require the full-scale materials to have physical thickness dimensions increased by a factor of $(p/p_o)^{2/3}$ from those of the model to insure a consistent thermally thick behavior. On the other hand, if all the materials happen to be thermally thin during flame spread at elevated pressures, extrapolation of the relative fire spread hazard to one atmosphere would not require any change in the physical dimensions of the materials.

The fact that the relative ranking of the NAFEC materials by upward spread growth factor appears to be insensitive to ambient pressure is somewhat fortuitous. Modeling theory, as noted before, predicts different pressure dependencies for spread rates on thermally thin and thermally thick materials. Both types of materials are likely to be represented by the NAFEC samples. However, the very large differences in spread rate among the samples tend to blur the detailed pressure dependencies and thereby preserve the ranking.

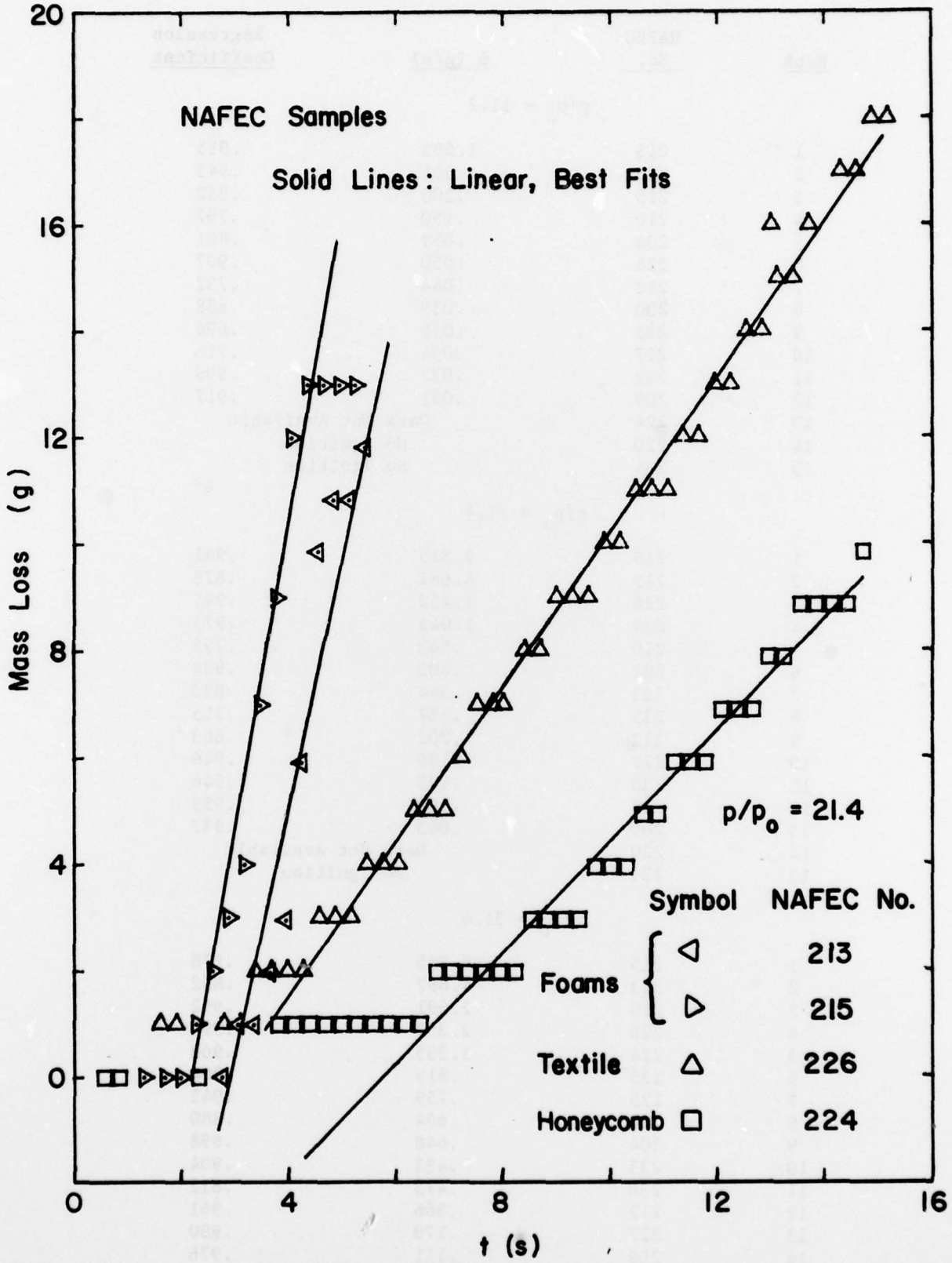

Figure 24: Examples of Fuel Mass Loss - Data acquisition begins at t=o, which roughly coincides with ignition of the sample.

Table 5. Peak Burning Rates of NAFEC Samples

Rank	NAFEC No.	$\dot{m}$ (g/s)	Regression Coefficient
		p/p_o = 11.2	
1	213	1.593	.915
2	226	.301	.943
3	215	.200	.862
4	210	.150	.797
5	204	.059	.861
6	225	.050	.907
7	212	.044	.732
8	230	.039	.888
9	235	.038	.696
10	227	.034	.716
11	233	.032	.599
12	209	.031	.917
13	224	Data Not Available	
14	220	No Ignition	
15	234	No Ignition	
		p/p_o = 21.4	
1	215	5.813	.961
2	213	4.681	.878
3	226	1.452	.991
4	224	1.045	.973
5	210	.543	.795
6	204	.402	.904
7	233	.344	.880
8	235	.337	.715
9	212	.202	.863
10	227	.136	.946
11	230	.105	.946
12	225	.103	.955
13	209	.043	.937
14	220	Data Not Available	
15	234	No Ignition	
		p/p_o = 31.6	
1	215	6.755	.978
2	213	4.897	.852
3	210	2.691	.962
4	226	2.357	.990
5	224	1.385	.968
6	235	.819	.804
7	225	.759	.945
8	220	.694	.880
9	204	.648	.898
10	233	.493	.904
11	230	.473	.812
12	212	.366	.961
13	227	.179	.980
14	209	.111	.976
15	234	No Ignition	

For thermally thin materials, spread rate should be independent of pressure, so the growth factor, V_f/x_f, should increase as $p^{2/3}$. Table 6 shows how the pressure-corrected growth factor, $(V_f/x_f)\ (p/p_o)^{-2/3}$, varies with ambient pressure for each of the 14 NAFEC materials which can be ignited. It is evident that in many cases, there is little variation in the corrected growth factor from 2.1 MPa to 3.16 MPa absolute pressure. Much larger variations are evident if the lowest pressure. 1.1 MPa, is included. However, upward spread rates are probably less reliable at this lower pressure, since flame spread is usually incomplete.

For thermally thick materials, V_f/x_f should increase as $p^{4/3}$, as explained previously. Table 7 shows how the pressure-corrected growth factor, $(V_f/x_f)\ (p/p_o)^{-4/3}$, is affected by the ambient pressure of the experiment. Again, for some materials, there is little variation in the corrected growth factor from 2.1 MPa to 3.16 MPa absolute pressure.

A comparison of these results from Table 6 and Table 7 shows that NAFEC materials 209, 212, 224, 226, 227, 233 and 235 are probably thermally thin during flame spread while NAFEC materials 213, 215, 225 and 230 are more nearly thermally thick during flame spread. The remaining 3 materials have a more complex thermal behavior.

Since the thermal wave thickness will greatly increase as pressure is reduced to one atmosphere, those materials which are thermally thin during flame spread on the model should remain thermally thin at full scale. The magnitude of flame spread growth factor at one-atmosphere for the thermally thin materials is then given directly by the values in Table 6 in the 21 or 31 atm. columns. Ranking of these thermally thin materials by decreasing growth factor at one-atmosphere would be the same as that shown in Table 3 since the same $(p/p_o)^{-2/3}$ factor has been applied to each growth factor. It is of interest to note that although NAFEC sample 209 would have the smallest growth factor (about $3.5 \times 10^{-3}\ s^{-1}$) of the thermally thin materials at one-atmosphere, thermally thick PMMA would have a slightly lower growth factor for upward spread at one-atmosphere ($2.4 \times 10^{-3}\ s^{-1}$).

Unfortunately, materials which are thermally thick during flame spread at elevated pressure (see Table 7) will not necessarily remain thermally thick as pressure is reduced due to the increased thermal wave thickness. Extrapolation of the upward spread results to full-scale would therefore not be at all reliable for such materials since the growth factor will not vary continuously as $(p/p_o)^{4/3}$ down to one-atmosphere. However, a "conservative" estimate of fire spread hazard at one-atmosphere could be obtained by assuming that the thermally thick materials change over to thermally thin behavior as pressure is reduced, with the growth factor then varying as $(p/p_o)^{2/3}$. The growth factors listed in Table 6 rather than Table 7 would thus characterize upward spread rates at one-atmosphere.

As shown in the first part of this report, the accuracy of the pressure modeling technique for thermally thick fuel beds depends mainly on the behavior of the net heat flux from the spreading flame to the fuel as a function of pressure. The upward spread velocity for thermally thin fuels also depends on this net flux, $\dot{q}''$, in the following manner described in reference 4:

Table 6. Upward Spread Growth Factors: Pressure Correction For NAFEC Samples Assumed Thermally Thin

$(V_f/x_f)(p/p_o)^{-2/3}$ (s^{-1})

NAFEC No.	p/p_o = 11.2	p/p_o = 21.4	p/p_o = 31.6	% Difference Last 2 Columns
204	1.66E-02*	1.50E-02	9.48E-03	37
209		3.80E-03	3.16E-03	17
210	2.02E-02	1.71E-02	2.86E-02	40
212	1.25E-02	9.21E-03	9.86E-03	7
213	8.33E-02	1.82E-01	2.66E-01	32
215	3.48E-02	1.16E-01	1.78E-01	35
220		7.09E-03	5.14E-03	28
224	1.15E-02	2.80E-02	2.73E-02	2
225	6.55E-03	4.85E-03	7.75E-03	37
226	3.87E-02	6.80E-02	5.71E-02	16
227	1.84E-02	8.91E-03	9.16E-03	3
230	9.47E-03	6.67E-03	8.21E-03	19
233	1.62E-02	1.44E-02	1.57E-02	8
235	4.26E-03	5.43E-03	6.10E-03	11

*E-02 = 10^{-2}

Table 7. Upward Spread Growth Factors: Pressure Correction For NAFEC Samples Assumed Thermally Thick

NAFEC No.	$(V_f/x_f)(p/p_o)^{-4/3}$ (s^{-1}) $p/p_o = 11.2$	$p/p_o = 21.4$	$p/p_o = 31.6$	% Difference Last 2 Columns
204	3.32E-03*	1.94E-03	9.48E-04	51
209		4.92E-04	3.16E-04	36
210	4.03E-03	2.21E-03	2.87E-03	23
212	2.49E-03	1.20E-03	9.86E-04	18
213	1.66E-02	2.36E-02	2.66E-02	11
215	6.95E-03	1.51E-02	1.78E-02	15
220		9.19E-04	5.14E-04	44
224	2.29E-03	3.63E-03	2.73E-03	25
225	1.31E-03	6.29E-04	7.76E-04	19
226	7.74E-03	8.82E-03	5.71E-03	35
227	3.68E-03	1.16E-03	9.16E-04	21
230	1.89E-03	8.65E-04	8.21E-04	5
233	3.24E-03	1.87E-03	1.57E-03	16
235	8.51E-04	7.05E-04	6.10E-04	13

*E-03 = 10^{-3}

$$V_p = \frac{C x_p \dot{q}'' \ln (x_f/x_p)}{d_s (T_p - T_\infty)} \qquad (9)$$

where C is a constant for a given fuel and d_s is the thickness of the fuel. Clearly, the dependence of the spread rate on $\dot{q}''$ is weaker for the thermally thin fuel than for the thermally thick case so errors in modeling the net flux are less critical.

An illustration of the effect of pressure on the dimensionless growth factor for thermally thin materials may be obtained from equation (9) by using the previously discussed properties of the PMMA flame and fuel surface. Fuel thickness, d_s, is held constant, as in the present experiments with aircraft materials. The result of such a calculation is shown in Figure 25 as the curve for T_{po} = 636 K, the reference pyrolysis temperature of PMMA fuel at one atmosphere. Values used for α and x_p are those which give the best agreement with experiment for thermally thick PMMA. It can be seen that modeling accuracy is rather uniform over a wide pressure range. Furthermore, it is likely that pressure modeling will lead to overestimates of upward spread rates at one atmosphere, rather than underestimates, for this case of thermally thin PMMA.

Curves are also shown in Figure 25 for higher and lower fuel pyrolysis temperatures, which might be characteristic of materials other than PMMA. At high ambient pressures, near p/p_o = 30 to 40, such changes in T_p do not have a strong effect on modeling accuracy.

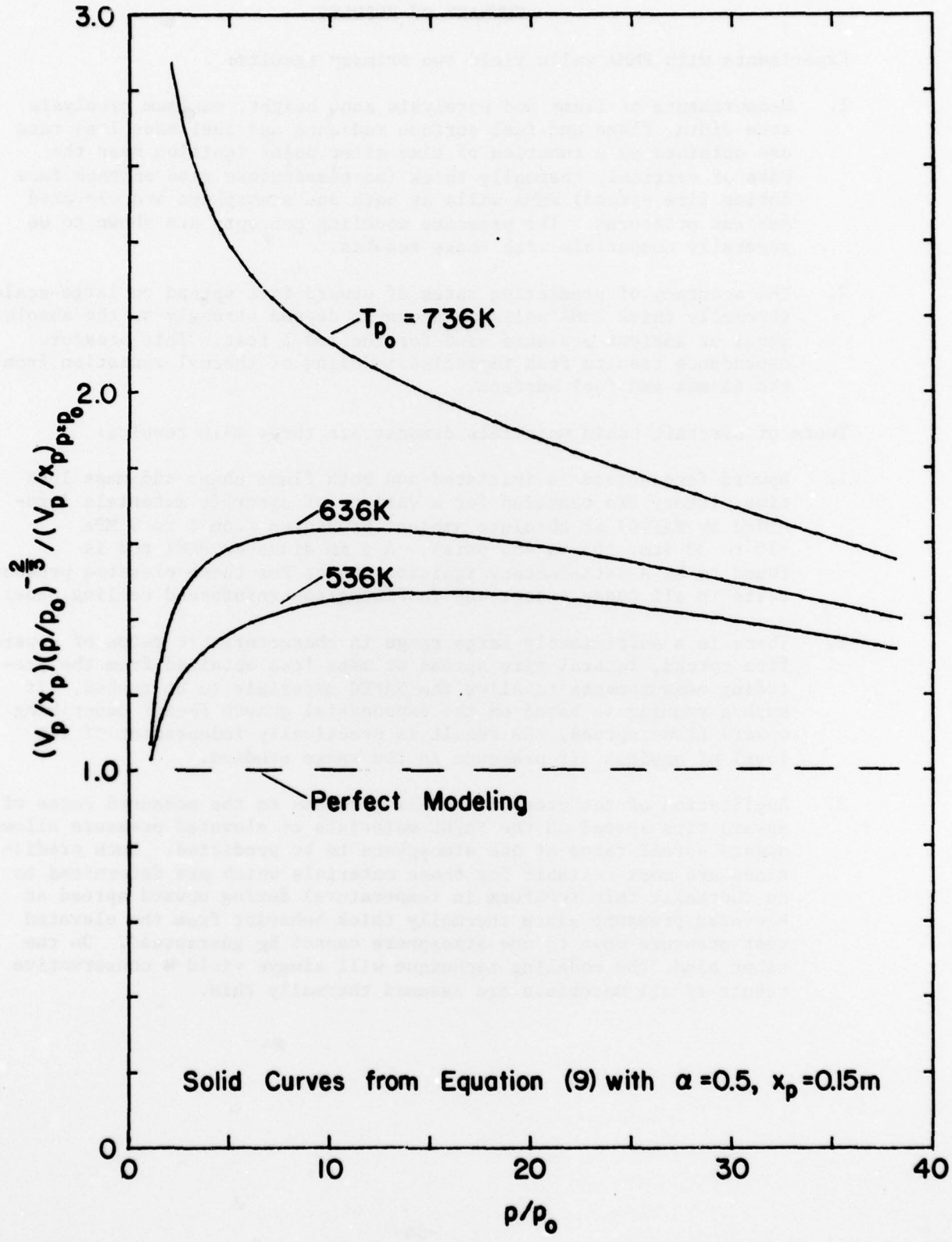

Figure 25: Predicted Exponential Growth Factor for Thermally Thin Materials

SUMMARY OF RESULTS

Experiments with PMMA walls yield two primary results:

1. Measurements of flame and pyrolysis zone height, maximum pyrolysis zone width, flame and fuel surface radiance and fuel mass loss rate are obtained as a function of time after point ignition near the base of vertical, thermally thick (no temperature rise on back face during fire spread) PMMA walls at both one atmosphere and elevated ambient pressures. The pressure modeling concepts are shown to be generally compatible with these results.

2. The accuracy of predicting rates of upward fire spread on large-scale, thermally thick PMMA walls is shown to depend strongly on the absolute level of ambient pressure used for the model test. This pressure dependence results from imprecise modeling of thermal radiation from the flames and fuel surface.

Tests of aircraft cabin materials demonstrate three main results:

1. Upward fire spread is initiated and both flame shape and mass loss time history are measured for a variety of aircraft materials (provided by NAFEC) at absolute ambient pressures from 1 to 3 MPa (10 to 30 atm, 165 to 465 psia). A 6 mm diameter PMMA rod is found to be a satisfactory ignition source for these elevated pressure tests in all cases except one (a fiberglass-reinforced ceiling panel).

2. There is a sufficiently large range in characteristic rates of upward fire spread, lateral fire spread or mass loss obtained from the preceding measurements to allow the NAFEC materials to be ranked. If such a ranking is based on the exponential growth factor describing upward flame spread, the result is practically independent of the level of ambient air pressure in the range studied.

3. Application of the pressure modeling scheme to the measured rates of upward fire spread on the NAFEC materials at elevated pressure allows upward spread rates at one atmosphere to be predicted. Such predictions are most reliable for those materials which are determined to be thermally thin (uniform in temperature) during upward spread at elevated pressure since thermally thick behavior from the elevated test pressure down to one atmosphere cannot be guaranteed. On the other hand, the modeling technique will always yield a conservative result if all materials are assumed thermally thin.

CONCLUSIONS

1. The pressure modeling technique is a valid method for prediction of upward fire spread behavior on vertical PMMA fuel walls several meters in height at one atmosphere.

2. Pressure modeling shows greatest accuracy when models are tested at an absolute air pressure of 30 to 35 atmospheres, due to thermal radiation effects.

3. Exposure of small samples of aircraft materials to an ignition source at elevated ambient air pressure allows the materials to be conveniently ranked by characteristic rate of upward fire spread, with such a ranking being reasonably independent of absolute air pressure from 1 to 3 MPa (10 to 30 atm).

4. Conservative estimates of rates of upward fire spread on aircraft cabin materials at one atmosphere can be made on the basis of tests with small-scale models at elevated pressures, even if the physical thickness of the material is the same at elevated pressure and at one atmosphere.

REFERENCES

1. deRis, J., Kanury, A.M., Yuen, M.C., "Pressure Modeling of Fires," Fourteenth Symposium (International) on Combustion, The Combustion Institute, p. 1033, 1973.

2. Alpert, R.L., "Pressure Modeling of Fires Controlled by Radiation", Sixteenth Symposium (International) on Combustion, The Combustion Institute, p. 1489, 1977.

3. Alpert, R.L., "Pressure Modeling of Transient Crib Fires", Combustion Science and Technology, 15, p. 11, (1976).

4. Orloff, L., deRis, J., Markstein, G.H., "Upward Turbulent Fire Spread and Burning of Fuel Surfaces:, Fifteenth Symposium (International) on Combustion, The Combustion Institute, p. 183, 1974.

5. Modak, A.T., Croce, P.A., "Plastic Pool Fires", Combustion and Flame, 30, p. 251 (1977).

6. Alpert, R.L., "Radiative Properties of PMMA Wall Fires", Factory Mutual Research Corp., Technical Report, in progress.

7. Hansen, A. and Sibulkin, M., "Flame Spreading from a Point Source of Ignition on a Vertical Fuel Surface", Combustion Science and Technology, 9, p. 173, (1974).

8. Orloff, L., Modak, A.T., Alpert, R.L., "Burning of Large-Scale Vertical Surfaces", Sixteenth Symposium (International) on Combustion, The Combustion Institute, p. 1345, 1977.

9. Sibulkin, M., Kim, J., "The Dependence of Flame Propagation on Surface Heat Transfer: II. Upward Burning", Combustion Science and Technology, 17, p. 39, (1977).

10. Hottel, H.C., Sarofim, A.F., "Radiative Transfer", McGraw-Hill Book Company, New York, p. 278, 1967.

11. Tamanini, F., "A Numerical Model for the Prediction of Radiation-Controlled Turbulent Wall Fires", Seventeenth Symposium (International) on Combustion, The Combustion Institute, to be published, 1979.

12. Markstein, G.H., "Radiative Properties of Plastics Pool Fires", Seventeenth Symposium (International) on Combustion, The Combustion Institute, to be published, 1979.

13. Annamalai, K., Sibulkin, M. "Ignition and Flame Spread Tests of Cellular Plastics", submitted for publication to Journal of Fires and Flammability, (1978).

14. Fernandez-Pello, A.C, "Upward Laminar Flame Spread Under the Influence of Externally Applied Thermal Radiation", Combustion Science and Technology, 17, p. 87, (1977).